Proteins: Mechanism of Protein Folding

CHEM 430

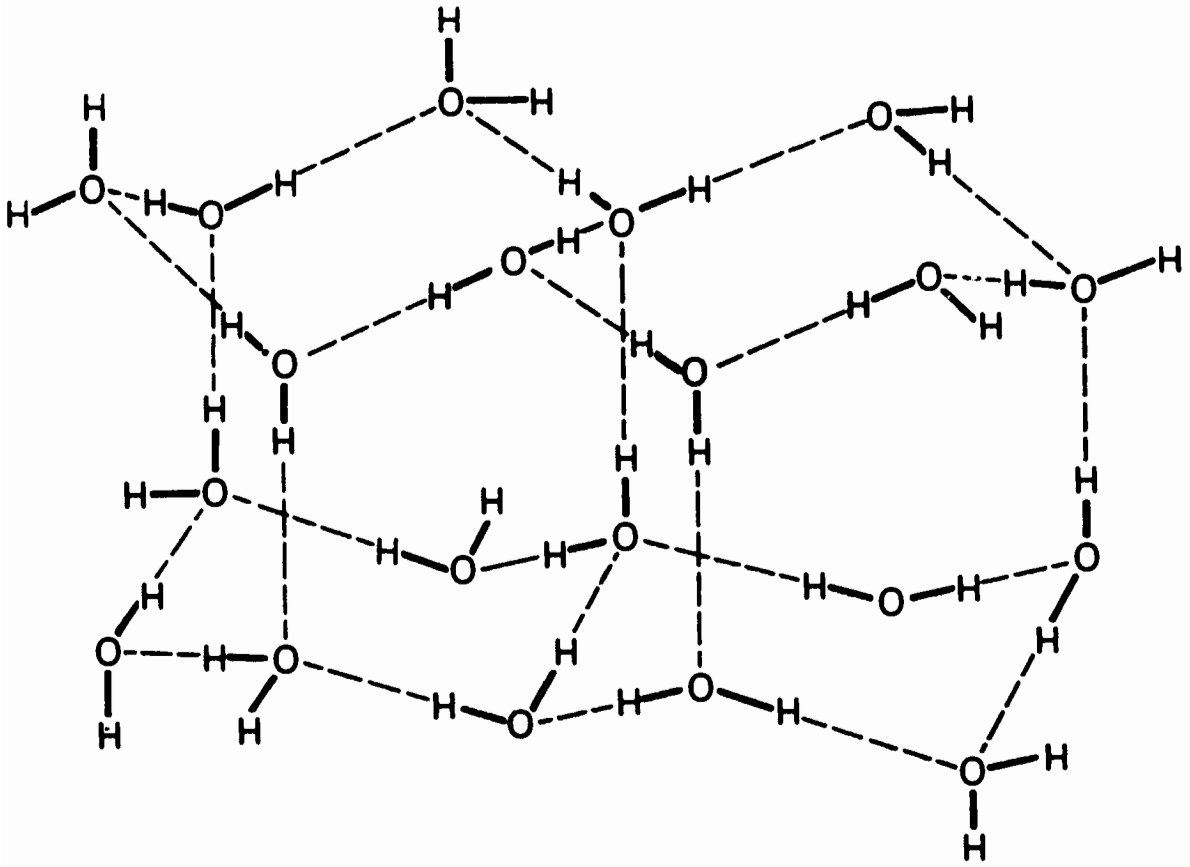

Figure 4–3
The structure of normal ice. Each H_2O molecule is involved in four hydrogen bonds, each 2.76 Å long, two as hydrogen donor and two as acceptor. As a consequence, substantial empty channels run between the molecules. (Adapted from F. H. Stillinger, Science 209:451–457, 1981.)

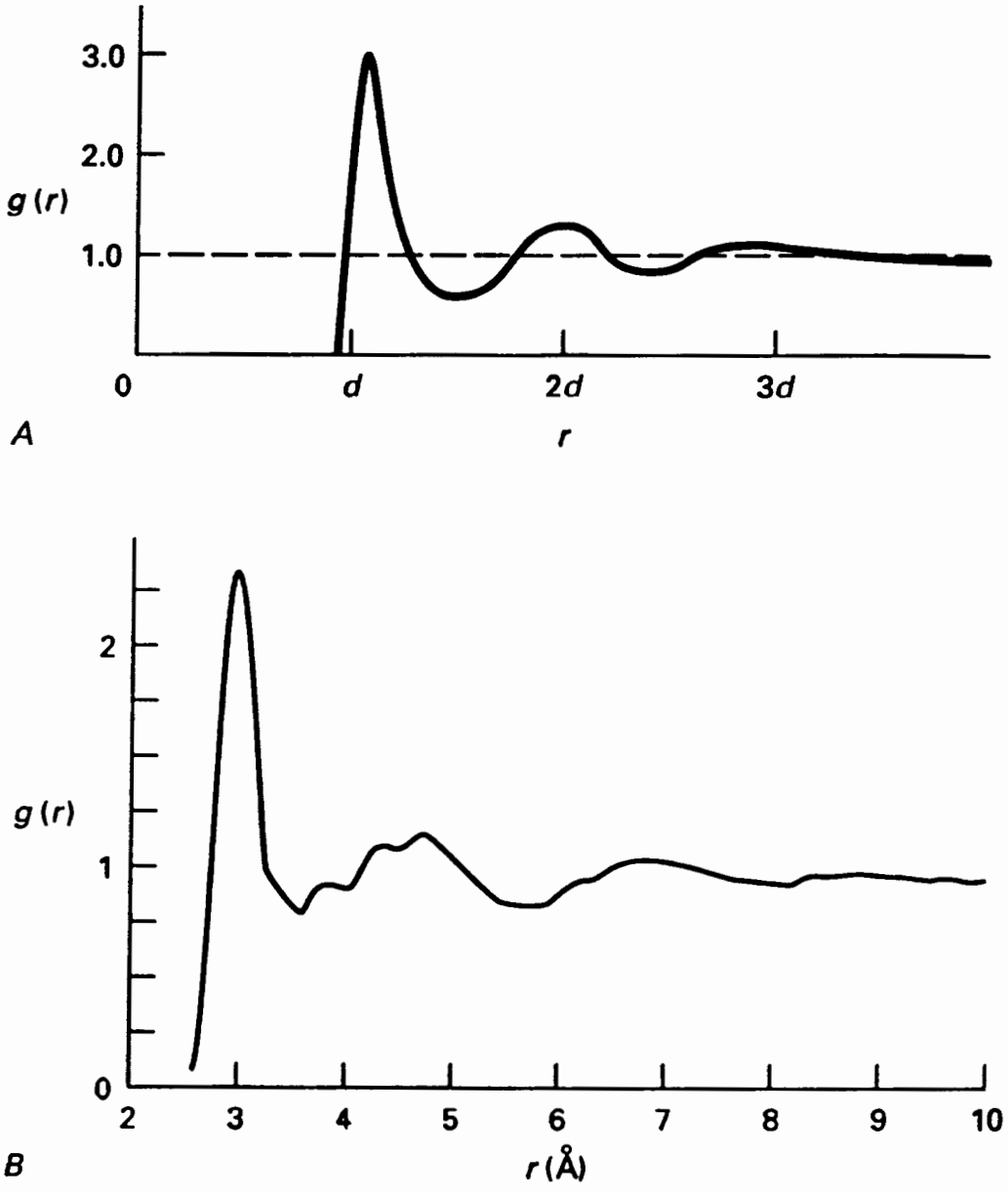

FIGURE 4.5

Radial distribution function of a normal liquid *(A)* and of water at 4°C *(B)*. The probability of finding other atoms at radial distance *r* from a central molecule is given by $g(r)$ times the density of the liquid. The distance *r* is expressed in *A* in terms of the van der Waals diameter of the molecule, *d*. The experimental curve for water measured using X rays is given in *B*; X rays are scattered primarily by the oxygen atom of the water molecule. (From A. H. Narten and H. A. Levy, *J. Chem. Phys.* 55:2263–2269, 1971.)

TABLE 4.2 Hydrated radii and hydration numbers of ions in water (approximate)

Ion	Bare ion radius (nm)	Hydrated radius (nm)	Hydration number (±1)	Lifetime (exchange rate) (s)
H_3O^+	—	0.28	3	—
Li^+	0.068	0.38	5–6	10^{-9}–10^{-8}
Na^+	0.095	0.36	4–5	10^{-9}
K^+	0.133	0.33	3–4	10^{-9}
Cs^+	0.169	0.33	1–2	10^{-10}–10^{-9}
Be^{2+}	0.031	0.46	4[a]	10^{-3}–10^{-2}
Mg^{2+}	0.065	0.43	6[a]	10^{-6}–10^{-5}
Ca^{2+}	0.099	0.41	6	10^{-8}
Al^{3+}	0.050	0.48	6[a]	10^{-1}–1
OH^-	0.176	0.30	3	
F^-	0.136	0.35	2	
Cl^-	0.181	0.33	1	
Br^-	0.195	0.33	1	
I^-	0.216	0.33	0	
NO_3^-	0.264	0.34	0	
$N(CH_3)_4^+$	0.347	0.37	0	

[a] Number of water molecules forming a stoichiometric complex with the ion (e.g., $[Be(H_2O)_4]^{2+}$). The hydration number gives the number of water molecules in the primary shell, though the total number of water molecules affected can be much larger and depends on the method of measurement. Similarly, the hydrated radius depends on how it is measured. Different methods can yield radii that can be as much as 0.1 nm smaller or larger than those shown. Table compiled from data given by Nightingale (1959), Amis (1975), Saluja (1976), Bockris and Reddy (1970), Cotton and Wilkinson (1980).

TABLE 3.2 Static dielectric constants[a] ε of some common liquids and solids at 25°C

Compound		ε	Compound	ε
Hydrogen bonding			*Polymers*	
Methyl formamide	$HCONHCH_3$	182.4	Nylon	3.7–4.2
Formamide	$HCONH_2$	109.5	Fluorocarbons	2.1–3.6
Hydrogen fluoride	HF (at 0°C)	84	Polycarbonate	3.0
Water	H_2O	78.5	Polystyrene	2.4
	D_2O	77.9	PTFE	2.0
Formic acid	HCOOH (at 16°C)	58.5	*Glasses*	
Ethylene glycol	$C_2H_4(OH)_2$	40.7	Fused quartz SiO_2	3.8
Methanol	CH_3OH	32.6	Soda glass	7.0
Ethanol	C_2H_5OH	24.3	Borosilicate glass	4.5
n-Propanol	C_3H_7OH	20.2	*Crystalline solids*	
Ammonia	NH_3	16.9	Diamond (carbon)	5.7
Acetic acid	CH_3COOH	6.2	Quartz SiO_2	4.5
			Micas	5.4–7.0
			Sodium chloride NaCl	6.0
			Alumina Al_2O_3	8.5
Non-hydrogen bonding				
Acetone	$(CH_3)_2CO$	20.7	*Miscellaneous*	
Chloroform	$CHCl_3$	4.8	Paraffin (liquid)	2.2
Benzene	C_6H_6	2.3	Paraffin wax (solid)	2.2
Carbon tetrachloride	CCl_4	2.2	Silicone oil	2.8
Cyclohexane	C_6H_{12}	2.0	Liquid helium (2–3 K)	1.055
Dodecane	$C_{12}H_{26}$	2.0	Water (liquid at 0°C)	87.9
Hexane	C_6H_{14}	1.9	Water (ice at 0°C)	91.6–106.4
			Air (dry)	1.00054

[a] The dielectric constant is a measure of the extent of reduction of electric fields and consequently of the reduced strengths of electrostatic interactions in a medium.

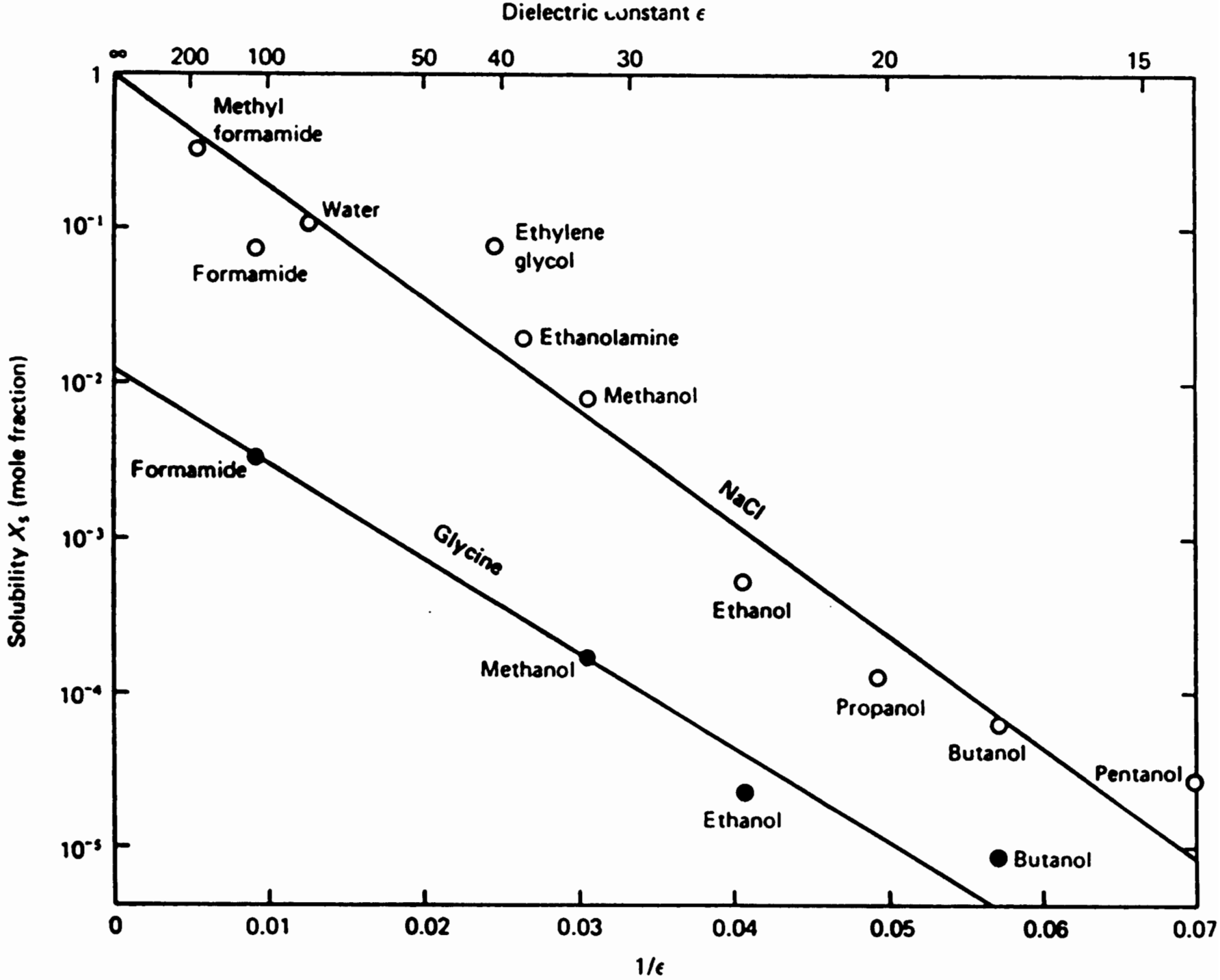
Dielectric constant ε
∞
200
100
50
40
30
20
15
1
10^{-1}
10^{-2}
10^{-3}
10^{-4}
10^{-5}
Solubility X_s (mole fraction)
Methyl formamide
Water
Formamide
Ethylene glycol
Ethanolamine
Methanol
NaCl
Formamide
Glycine
Ethanol
Methanol
Propanol
Butanol
Pentanol
Ethanol
Butanol
0
0.01
0.02
0.03
0.04
0.05
0.06
0.07
1/ε

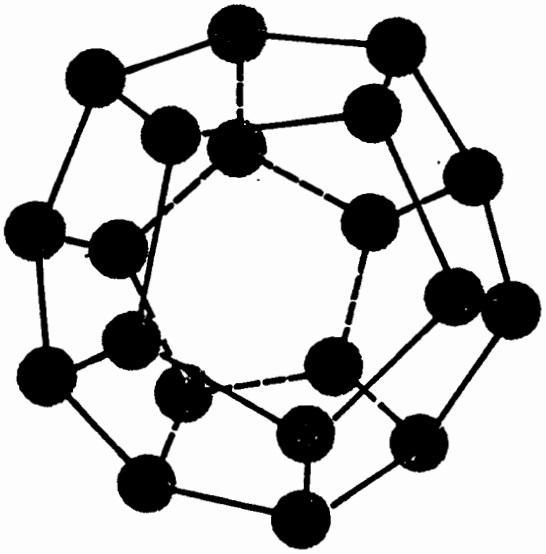

(a)

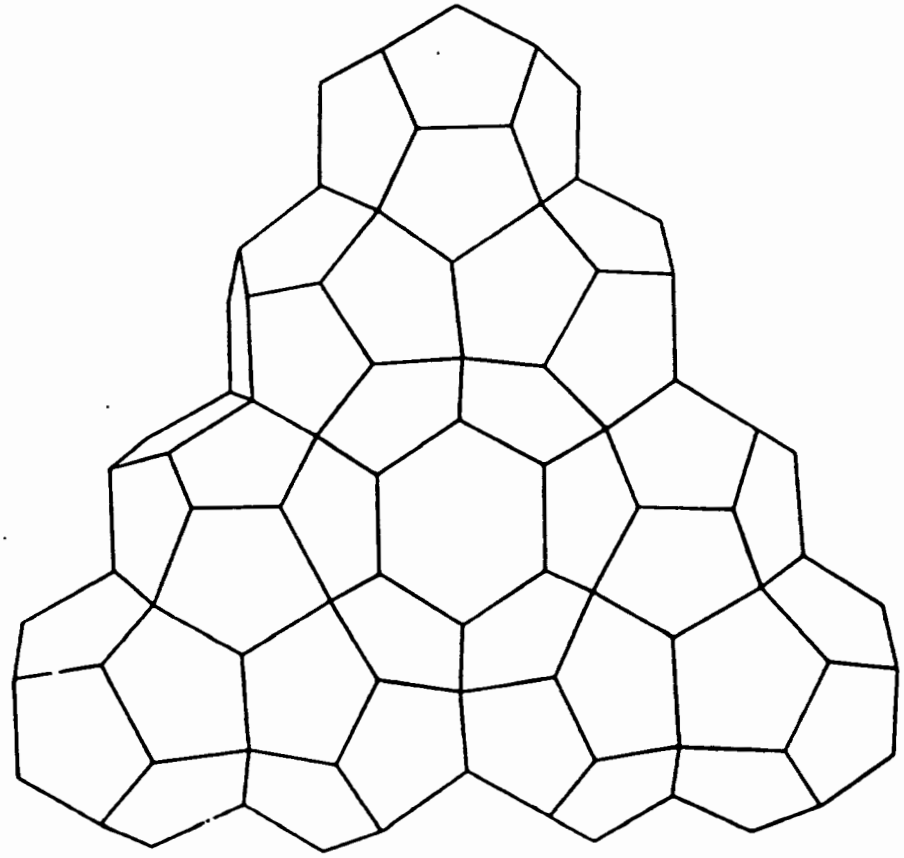

(b)

Figure 5-15

Pentagonal dodecahedrons. (a) Pentagonal dodecahedron formed by water molecules (balls) enclosing a cavity of ~5Å diameter.

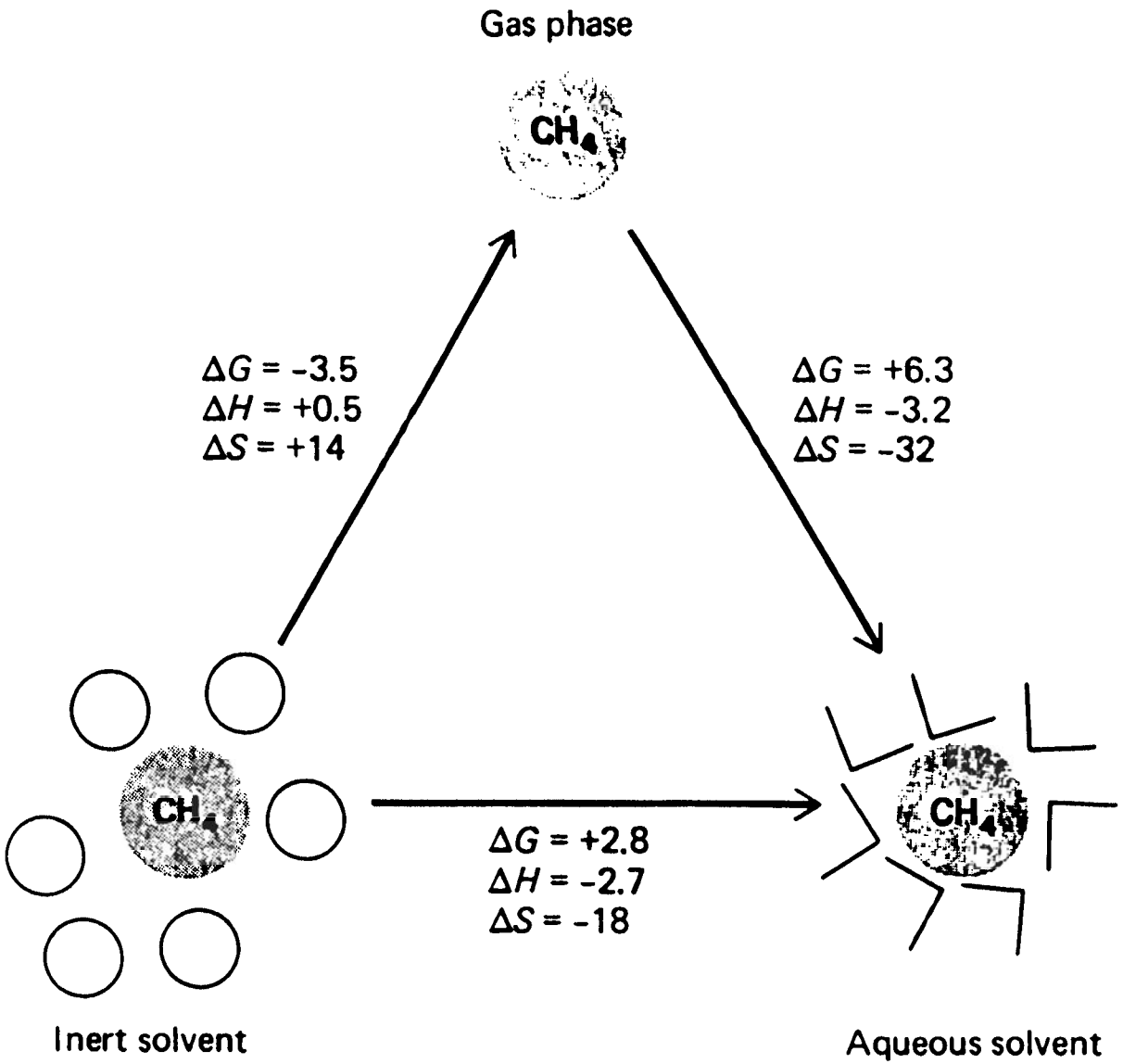

Figure 4–4

Thermodynamics of the hydrophobic effect. The transfer of one molecule of methane to water from an inert, nonpolar solvent, such as carbon tetrachloride, is illustrated both directly and through the gas phase. The changes in Gibbs free energy, ΔG, and in enthalpy, ΔH, are expressed in kcal/mole; those of entropy, ΔS, in entropy units, kcal/mole/°K. (Adapted from W. P. Jencks, Catalysis in Chemistry and Enzymology. New York, McGraw-Hill, 1969.)

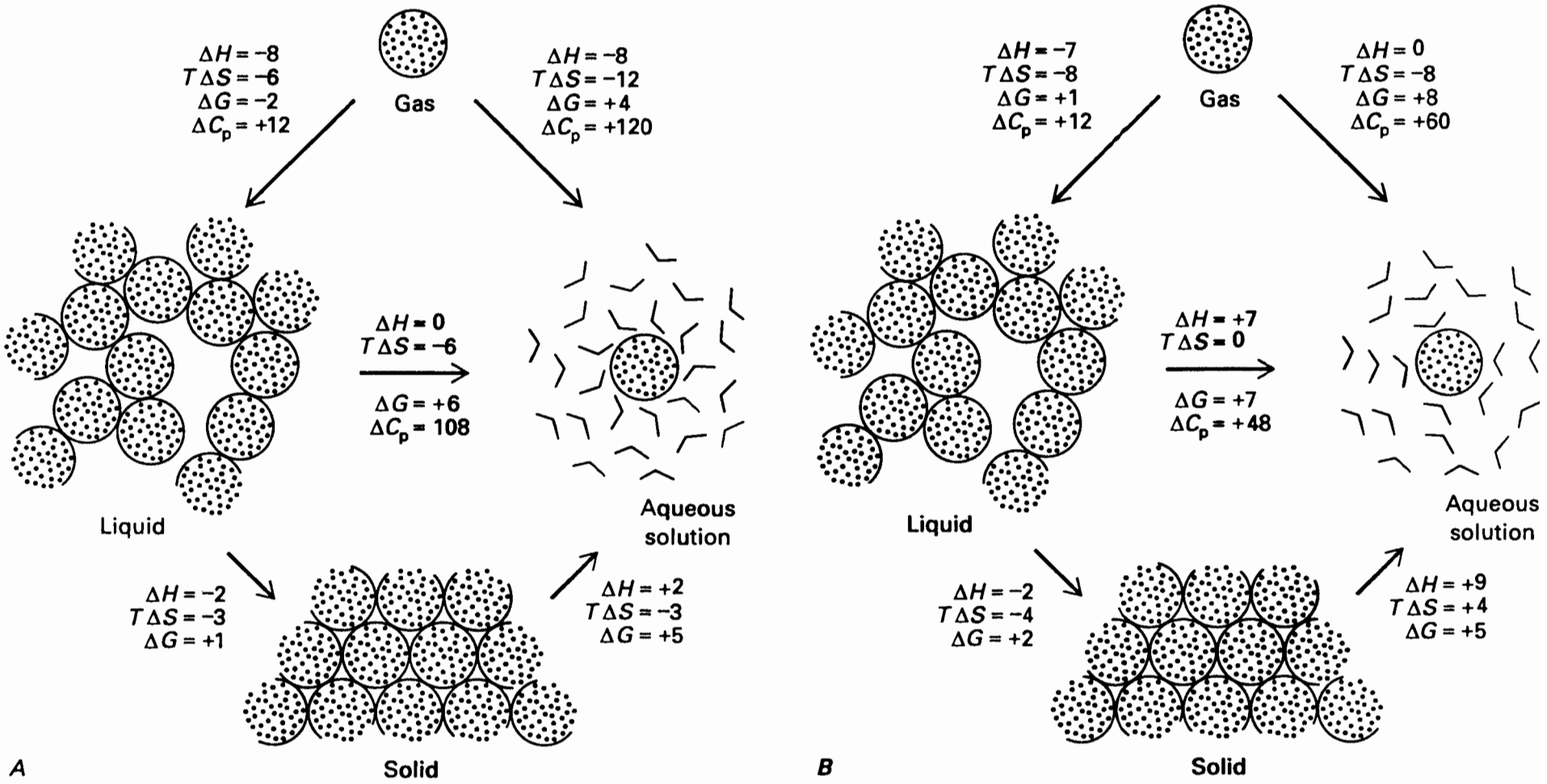

FIGURE 4.9

Typical thermodynamics of transfer of a nonpolar molecule the size of cyclohexane between the gas, liquid, and solid phases and aqueous solution at two temperatures: *(A)* T_H, approximately 20°C, where $\Delta H_{tr} = 0$ for transfer between liquid and water; and *(B)* T_S, approximately 140°C, where $\Delta S_{tr} = 0$. The values of ΔH, $T\Delta S$, and ΔG are in units of kcal/mol, that of ΔC_p in units of cal/(K·mol).

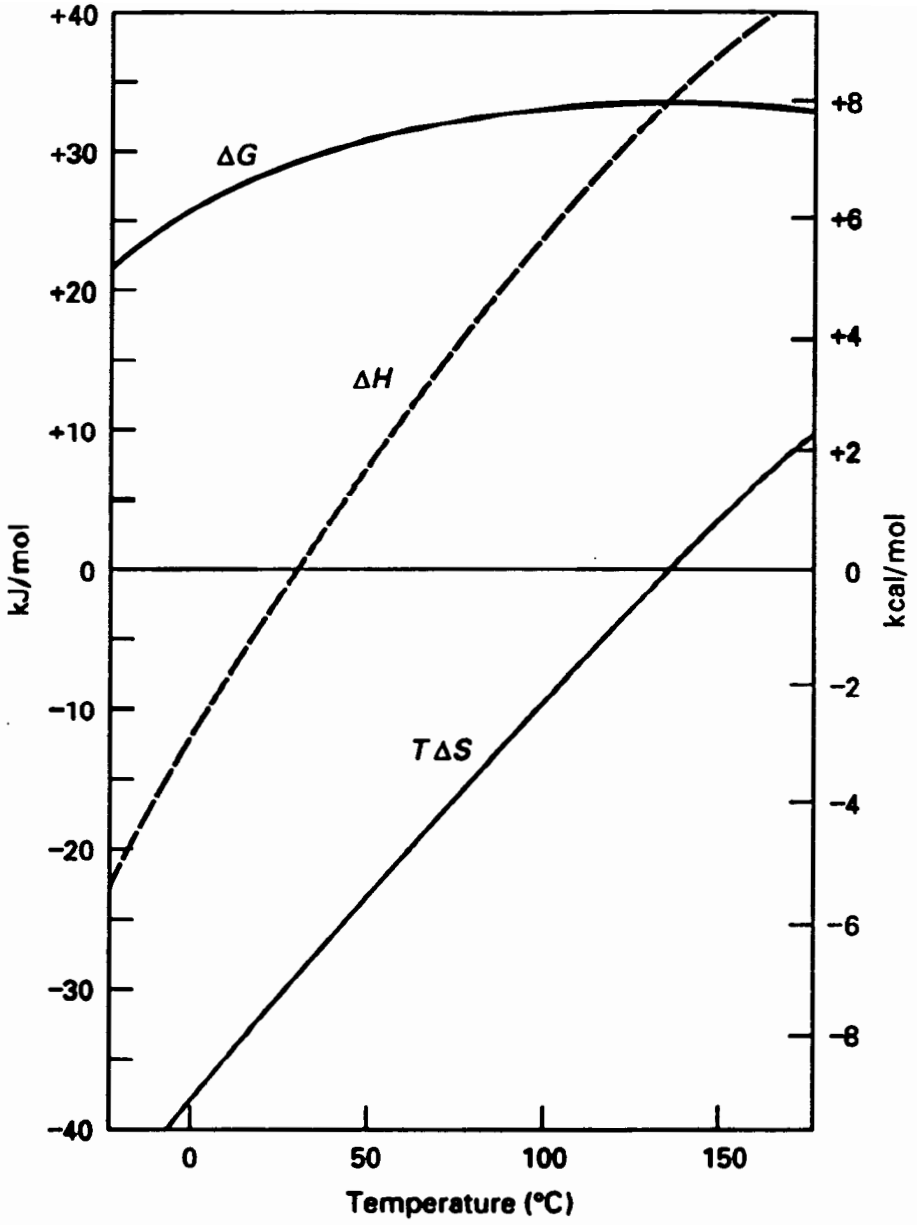

FIGURE 4.10

Typical thermodynamics of the free energy of transfer of a hydrocarbon from the liquid to aqueous solution, using pentane as an example. The strong temperature dependence of both the enthalpy and entropy difference between the two phases is a result of the different heat capacities of the two phases. The free-energy difference is the net difference between the enthalpic (ΔH) and entropic ($T\,\Delta S$) contributions. It reaches a maximum where $\Delta S = 0$, whereas the equilibrium constant (which is proportional to $-\Delta G/T$) reaches a maximum where $\Delta H = 0$. (Adapted from P. L. Privalov and S. J. Gill, *Adv. Protein Chem.* 39:191–234, 1988.)

TABLE 4-3 *Thermodynamic Changes for the Transfer of Hydrophobic Hydrocarbons from a Nonpolar Solvent to Water*[1]

PROCESS	TEMP/K	$\Delta S°$/CAL MOL^{-1}	$\Delta H°$/CAL MOL^{-1}	$\Delta G°$/CAL MOL^{-1}
CH_4 in benzene → CH_4 in H_2O	298	−18	−2800	+2600
CH_4 in ether → CH_4 in H_2O	298	−19	−2400	+3300
CH_4 in CCl_4 → CH_4 in H_2O	298	−18	−2500	+2900
C_2H_6 in benzene → C_2H_6 in H_2O	298	−20	−2200	+3800
Liquid benzene → C_6H_6 in H_2O	291	−14[2]	0	+4070[2]
Liquid toluene → C_7H_8 in H_2O	291	−16[2]	0	+4650[2]

TABLE 4-4 *Free-Energy Changes for Transfer of Amino Acids to Water at 25°C*[1]

AMINO ACID	$\Delta G°$/CAL MOL^{-1} FOR TRANSFER	$\Delta G°$/CAL MOL^{-1} FOR TRANSFER OF SIDE CHAIN
Glycine	−4630	(0)
Alanine	−3900	730
Valine	−2940	1690
Leucine	−2210	2420
Isoleucine	−1690	2970
Phenylalanine	−1980	2650
Proline	−2060	2600

TABLE 4-5 *Changes in Thermodynamic Quantities for Proteins During Denaturation*[1]

PROTEIN	CONDITIONS FOR DENATURATION	ΔG/KCAL MOL^{-1}	ΔH/KCAL MOL^{-1}	ΔS/CAL MOL^{-1} °C^{-1}	ΔC_p/CAL MOL^{-1} °C^{-1}
Ribonuclease	pH 2.5, 30°C	0.9	57	185	2000
Chymotrypsinogen	pH 3, 0.01M Cl^-, 25°C	7.3	39	105	2600
Myoglobin	pH 9, 25°C	13.6	42	95	1900
β-lactoglobulin	5M urea, pH 3, 25°C	0.6	−21	−72	2150

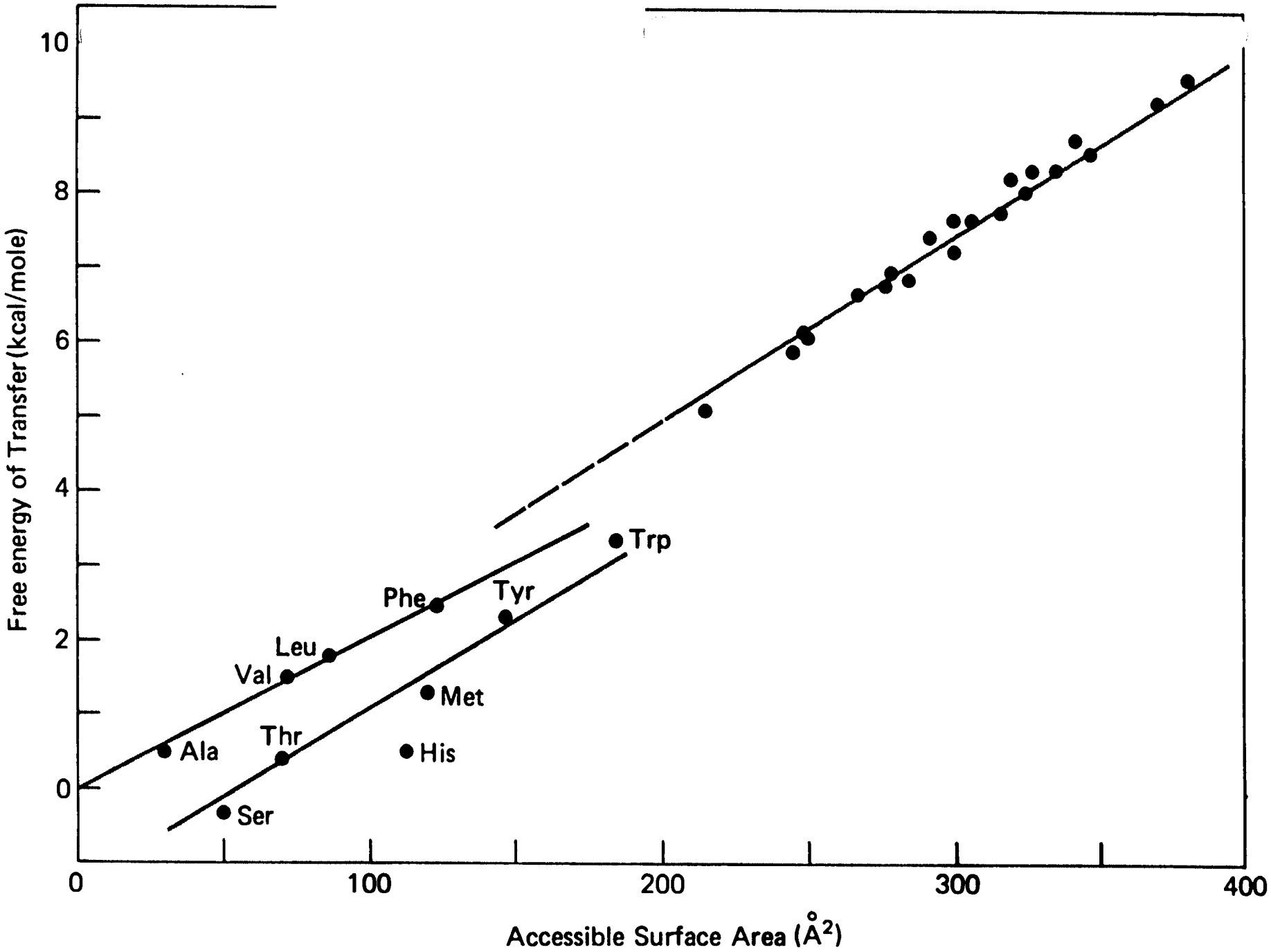

Figure 4–5

Correlation between hydrophobicity and accessible surface area. The unlabeled dots are for various hydrocarbons; the line extrapolates back to the origin and has a slope of 25 cal/Å².

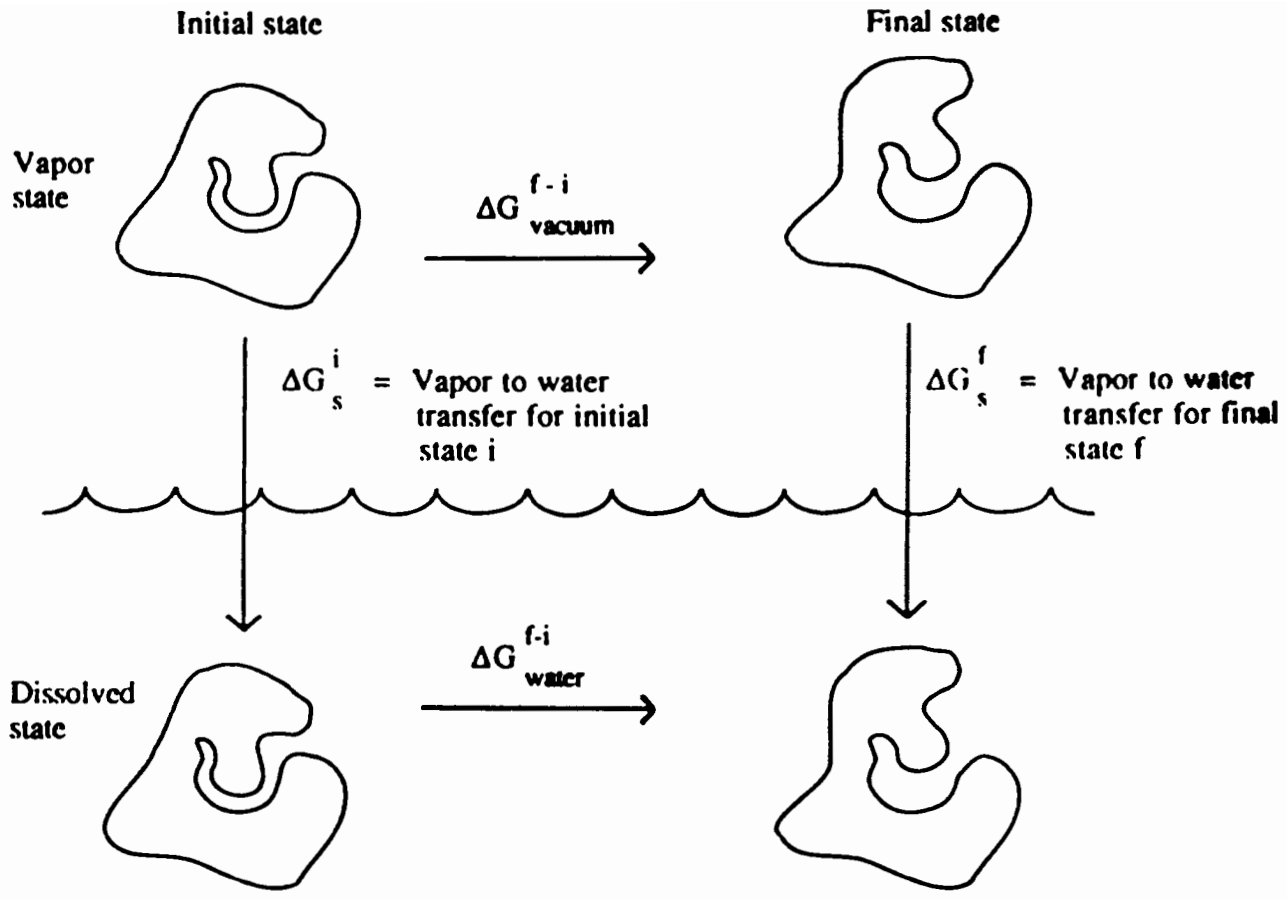

Fig. 1. Thermodynamic cycle that shows how vapor-to-water free energies of transfer may be used to compute protein free energy changes in solution. ΔG^{f-i}_{vacuum} is the free energy difference between two conformational states in vacuum, available in principle by molecular simulation. ΔG^{i}_{s} and ΔG^{f}_{s} are the vapor-to-water free energies of transfer for the protein in the initial and final conformational states. The free energy difference between the two conformational states in water, ΔG^{f-i}_{water}, may be calculated from the thermodynamic cycle.

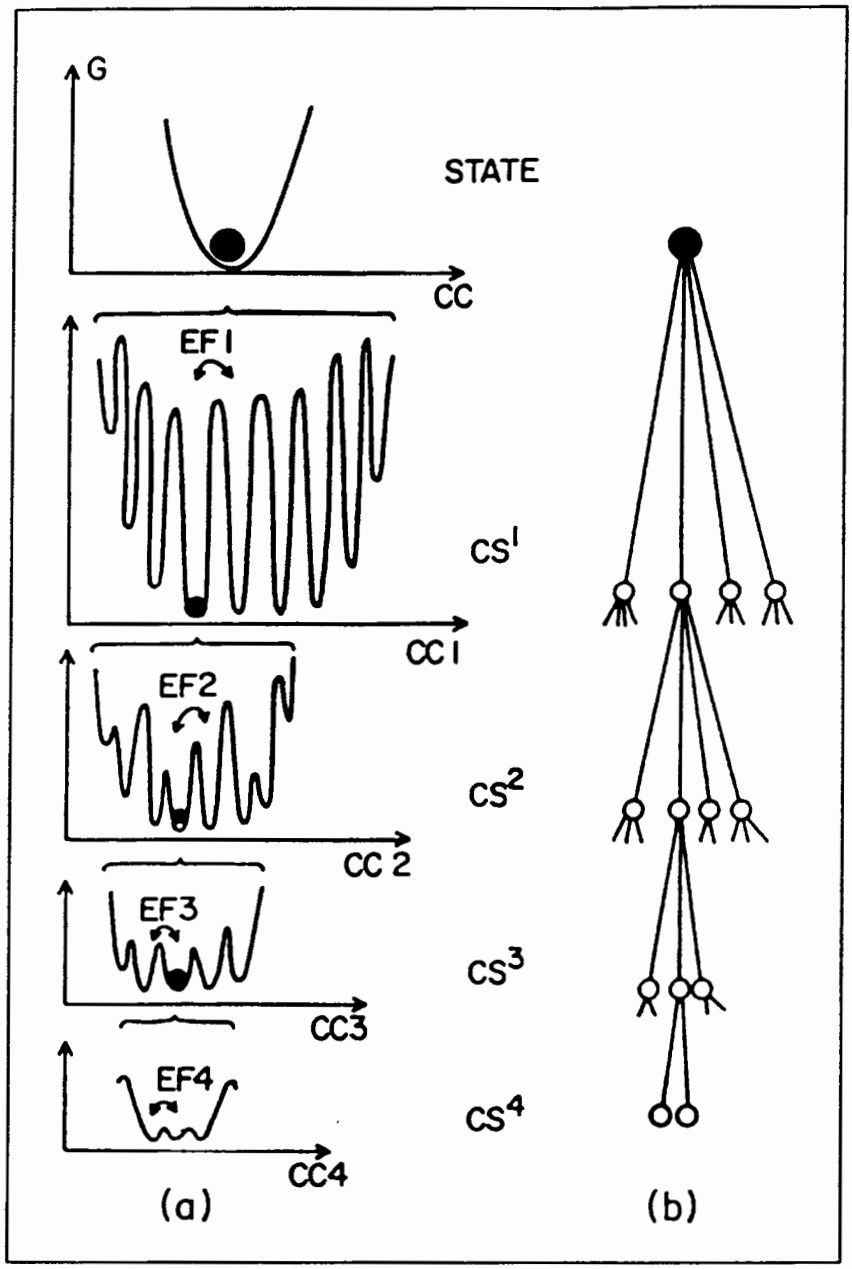

FIGURE 1–4. *Schematic diagram of conformational substates, CS, and equilibrium fluctuations, EF. The ordinate is the Gibbs free energy, the abscissae the conformational coordinates, CC 1–4. At room temperature the state CC appears to be located in a smooth well. As the temperature is lowered, the substructure of the energy landscape begins to appear with many minima representing closely similar forms in thermal equilibrium. As the temperature decreases, molecules are frozen into the individual minima, each of which develops additional structure. Within each tier of substates, the equilibrium fluctuations distribute the molecules among these minima. The final tier, CS^4, would be identifiable only at a temperature near absolute zero. This general description was set up to rationalize the data collected on the kinetics of the photodissociation and reassociation of the myoglobin-carbon monoxide complex as a function of temperature. (Reprinted with permission from Ansari et al., 1985)*

Mechanism of the Protein Folding Reaction

1. Levinthal Random Sampling
2. Sequential Folding Model
3. Nucleation/Growth Model
4. Diffusion–Collision–Adhesion
5. Framework Model
6. Hydrophobic Collapse Model
7. Jigsaw Puzzle Model

The elementary form of the folding reaction is deceptively simple:

denatured or unfolded — U ⇌ N — native or folded

renaturation or folding

denaturation or unfolding

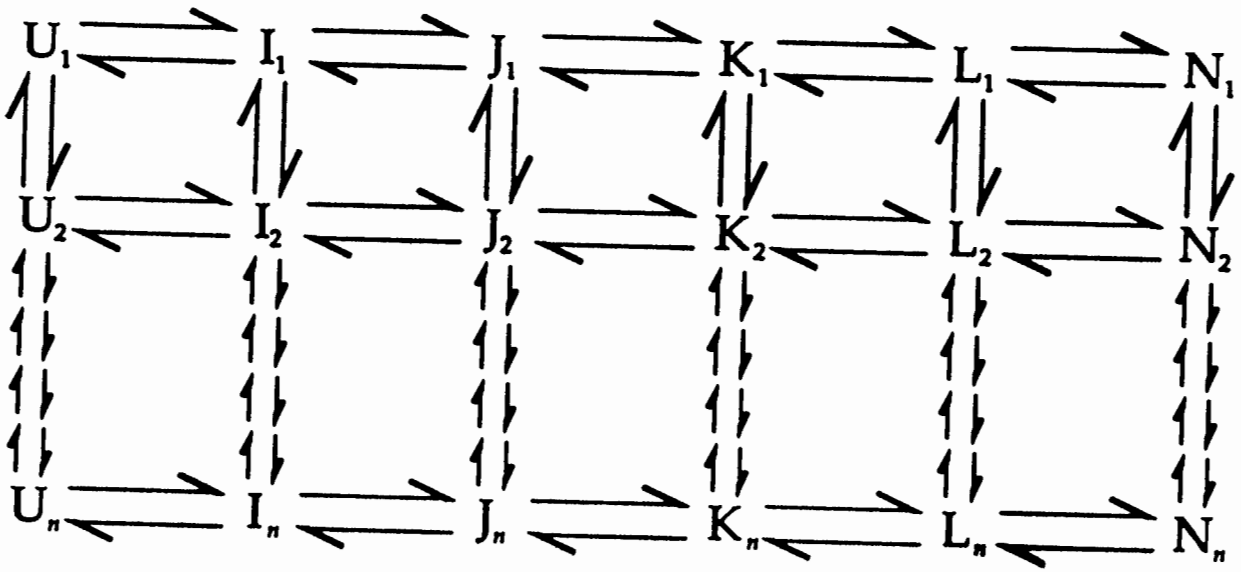

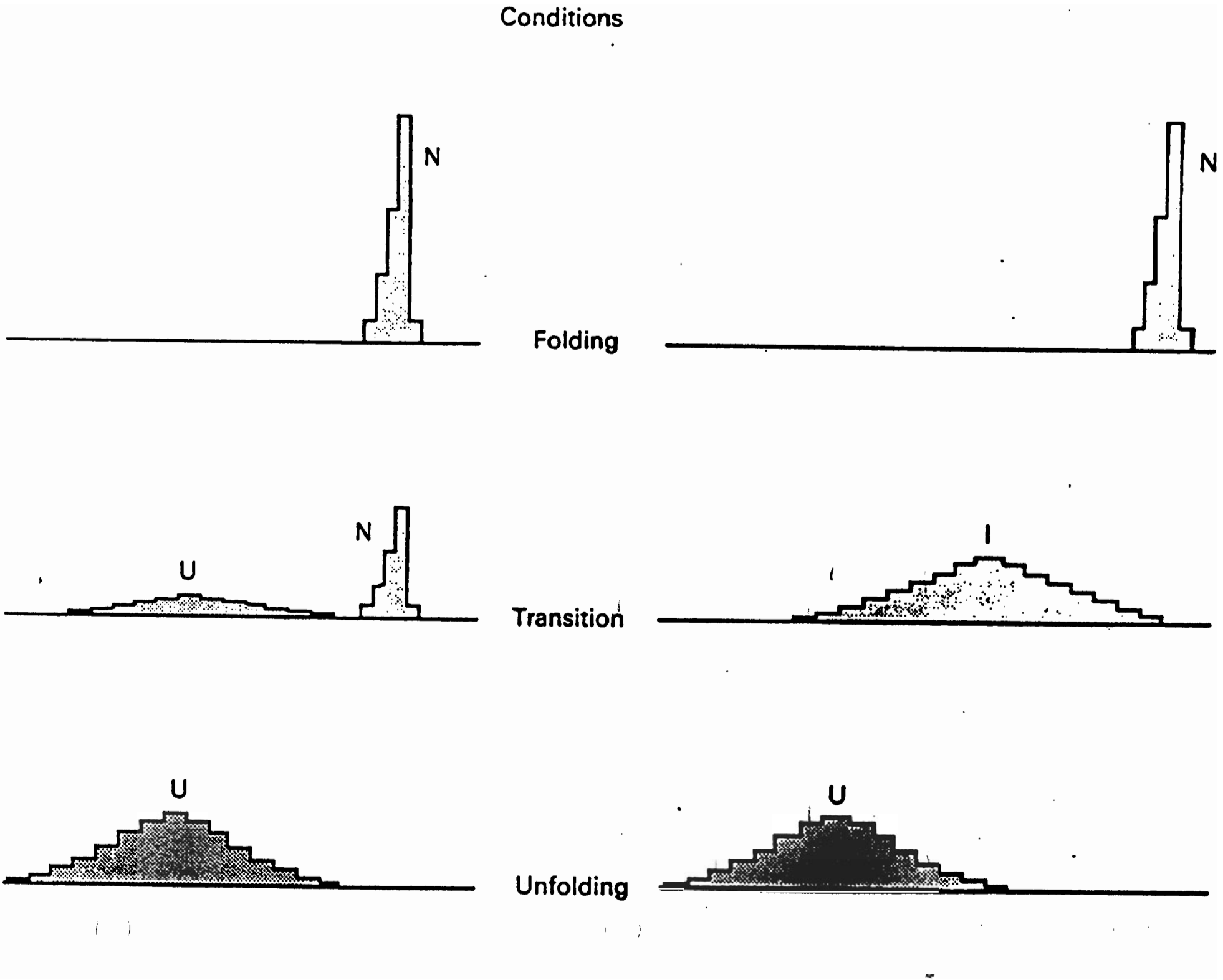
Conditions
N
N
Folding
N
U
I
Transition
U
U
Unfolding

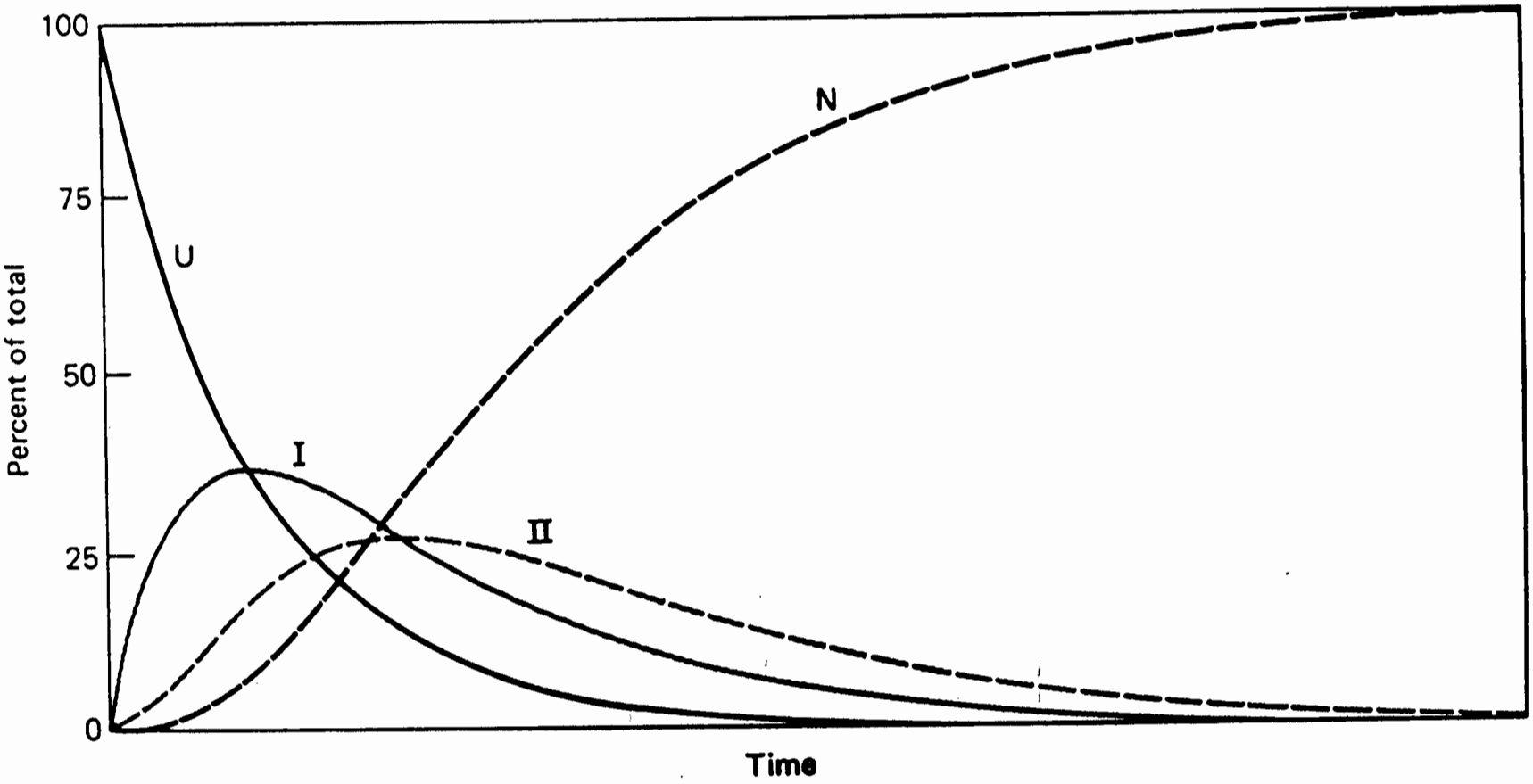

Kinetics of a three-step sequential reaction, $U \rightarrow I \rightarrow II \rightarrow N$, in which all three steps have the same rate constant. The intermediates accumulate to relatively low concentrations.

Fig. 4. Schematic illustration of co-operativity between two interactions, with equilibrium constants K_A and K_B in the unfolded polypeptide chain, U. If both interactions are possible simultaneously, the presence of one will increase the proximity of the other pair of groups, and less conformational entropy of the polypeptide chain will need to be lost for them to interact. Consequently, each interaction will be stronger when the other is also present by the factor 'Co-op'. The effect must be mutual, due to the thermodynamic requirement that there be no free energy change around such a cycle.

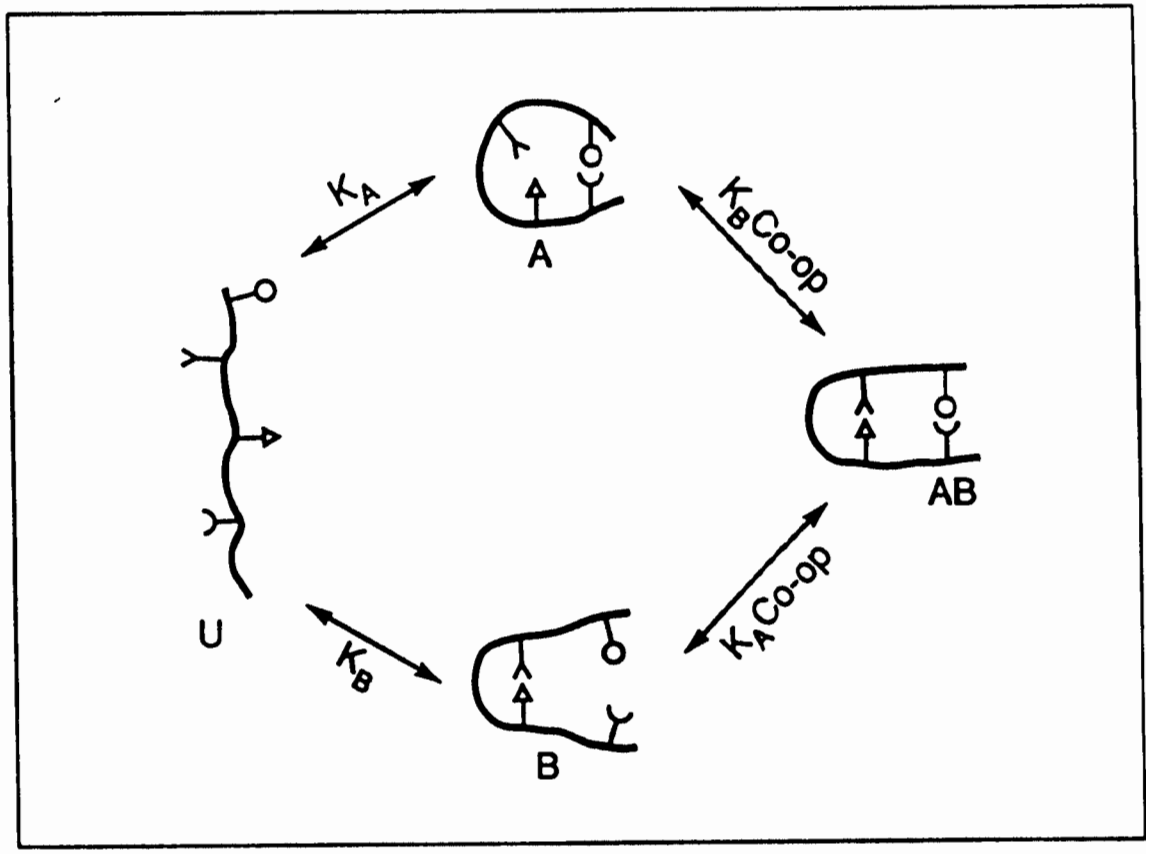

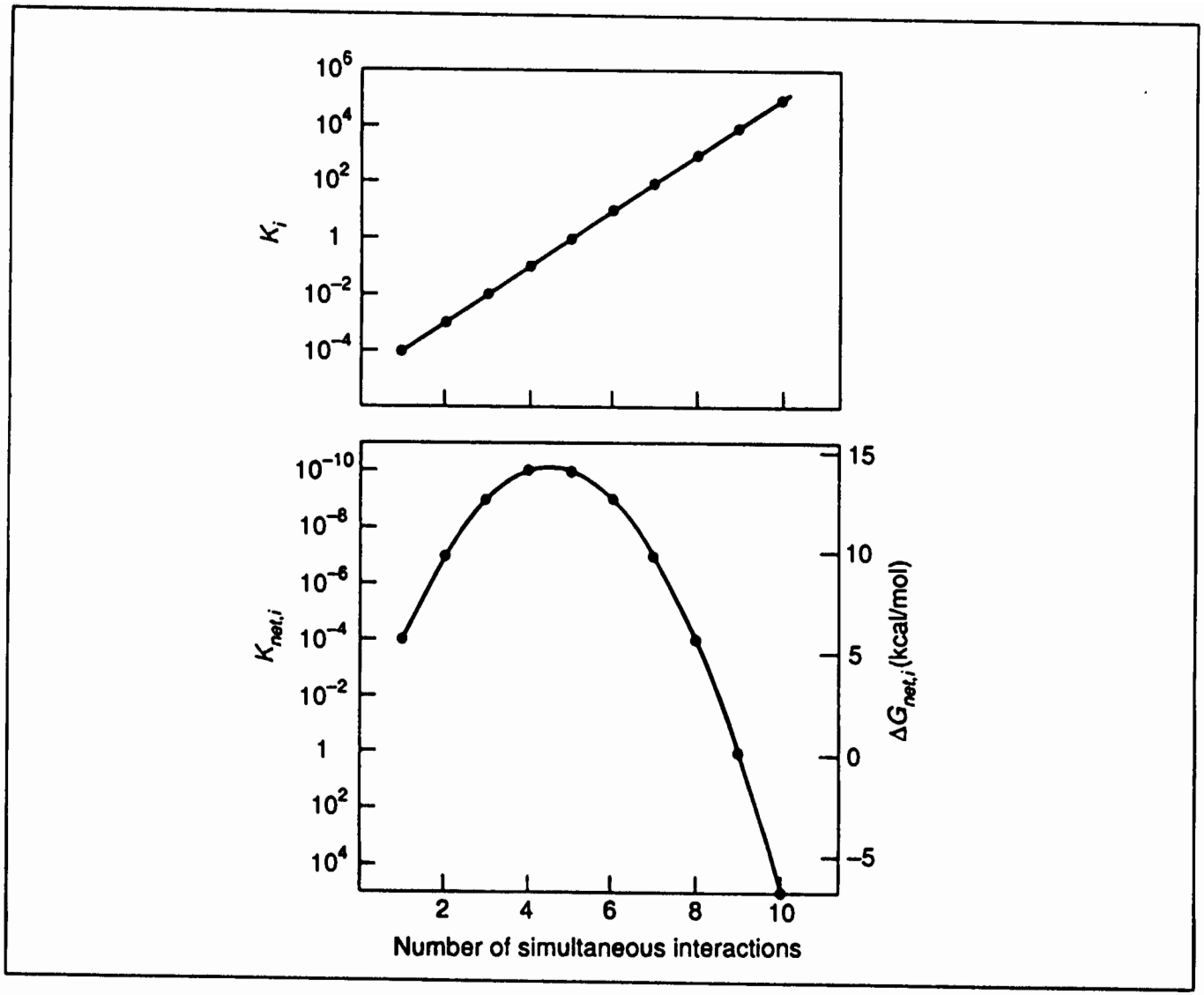

Fig. 5. Hypothetical illustration of the co-operativity of protein folding produced by multiple weak interactions. The equilibrium constant for forming the *i*th interaction, K_i, is shown at the *top*. Individual interactions are postulated to be weak in U, with equilibrium constants no greater than 10^{-4}; each interaction is postulated to be ten times stronger than the preceding one due to entropic co-operativity between them, as described in Fig. 4. The overall equilibrium constant between U with no interactions and each species with *i* interactions, $K_{net,i}$, is given at the *bottom*. The value of $K_{net,i}$ decreases initially, as each K_i is less than unity. As K_i becomes greater than unity, the value of $K_{net,i}$ increases. Only with 10 such interactions is $K_{net,i} > 1$ and the folded structure stable. The free energy of each state relative to U is given by $\Delta G_{net,i} = -RT \ln K_{net,i}$, with the scale on the *right* pertaining to 25 °C.

(a)

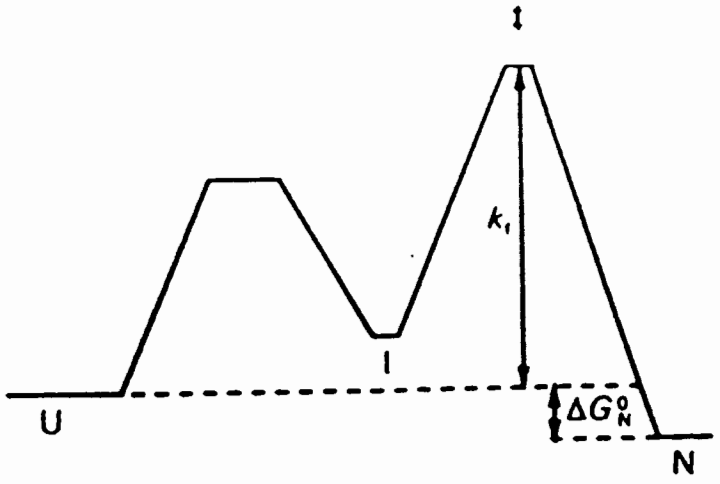

(b)

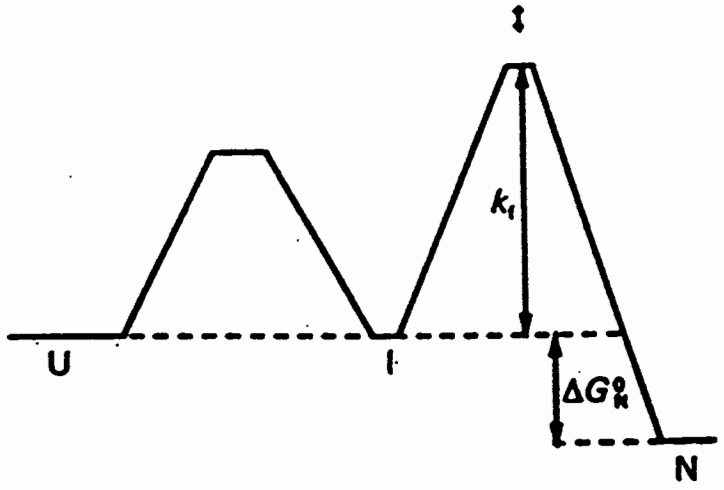

(c)

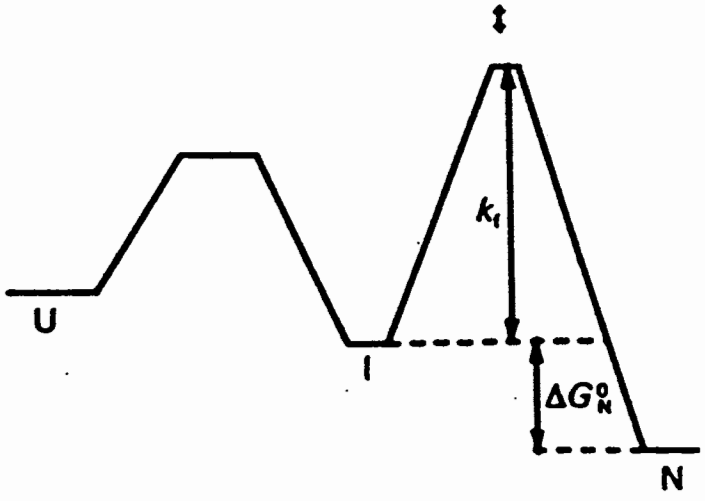

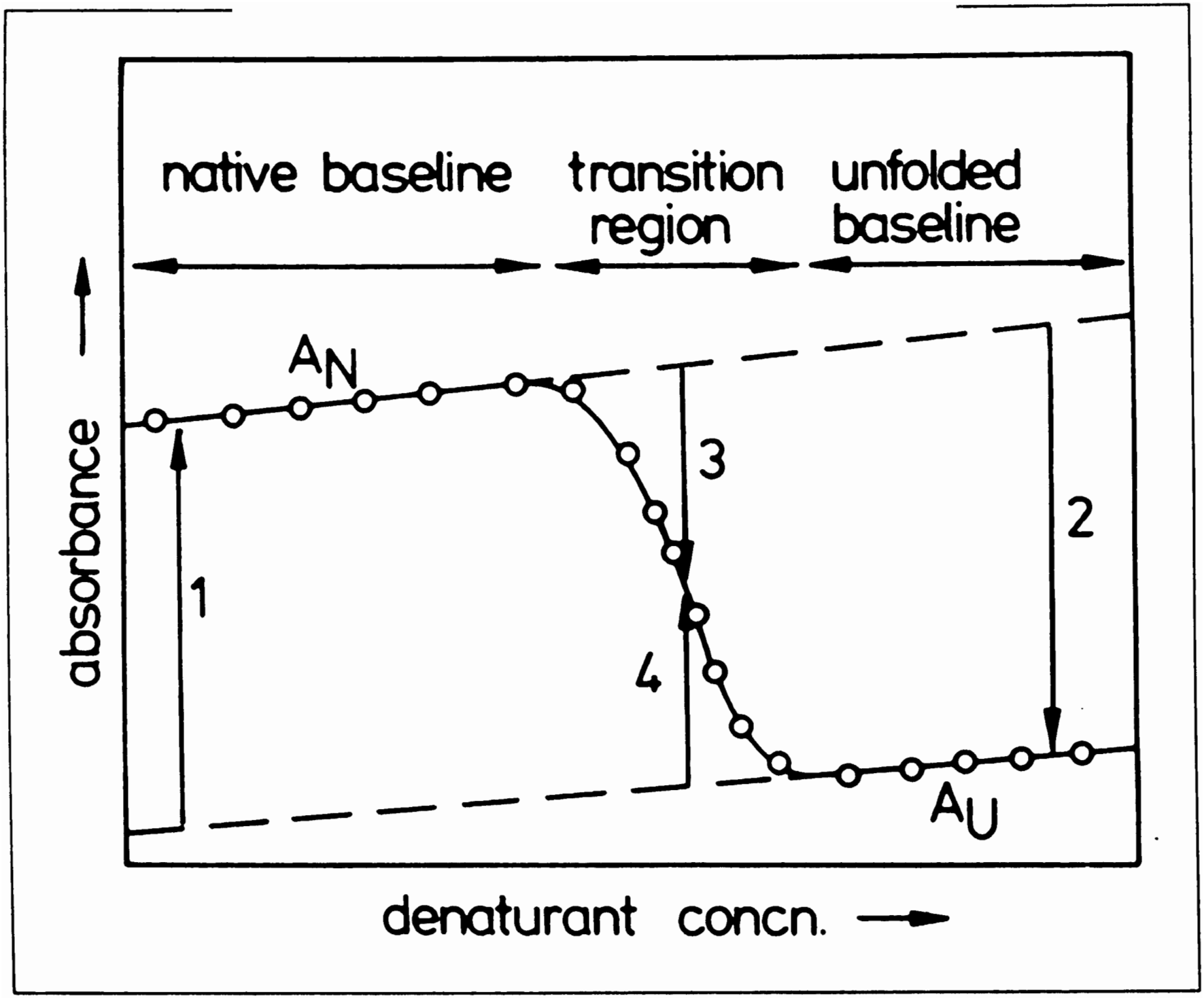

FIGURE 5–1. Schematic representation of a denaturant-induced unfolding transition

(A) Schematic unfolding transition.

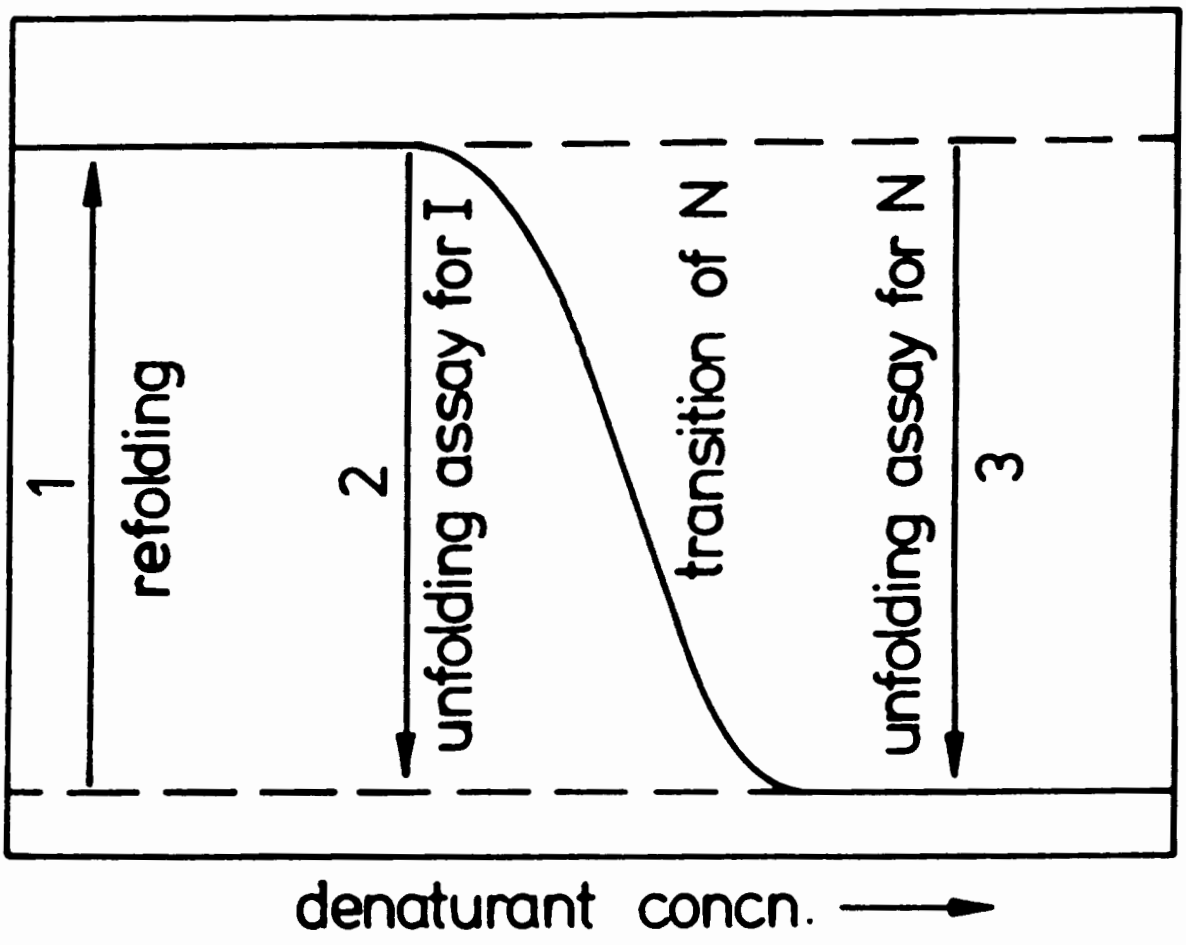

(B) Two-step procedure:

I: Refolding step.
At t = 0 : Start refolding in a test tube (cf. arrow 1)

II: Unfolding assay.
At $t = t_i$: jump to (2) or (3) to measure, respectively, the unfolding amplitude of the intermediate (I) or the native protein (N), as indicated by arrows (2) and (3).

FIGURE 5–5. Schematic outline of the method of using unfolding assays to measure the formation of intermediates or of native protein during refolding.

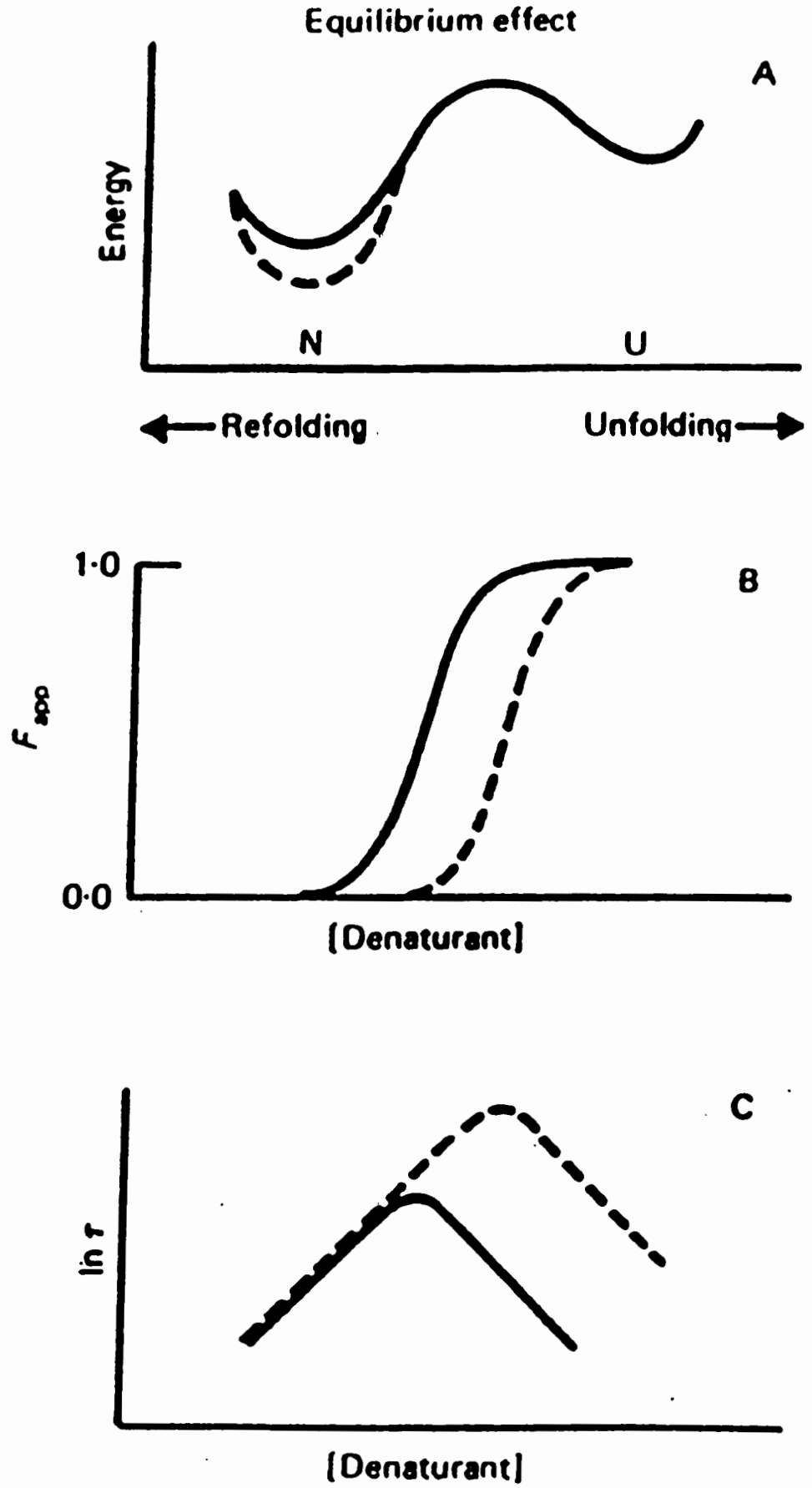
Equilibrium effect
A
Energy
N
U
Refolding
Unfolding
1·0
0·0
F_{app}
B
[Denaturant]
C
ln r
[Denaturant]

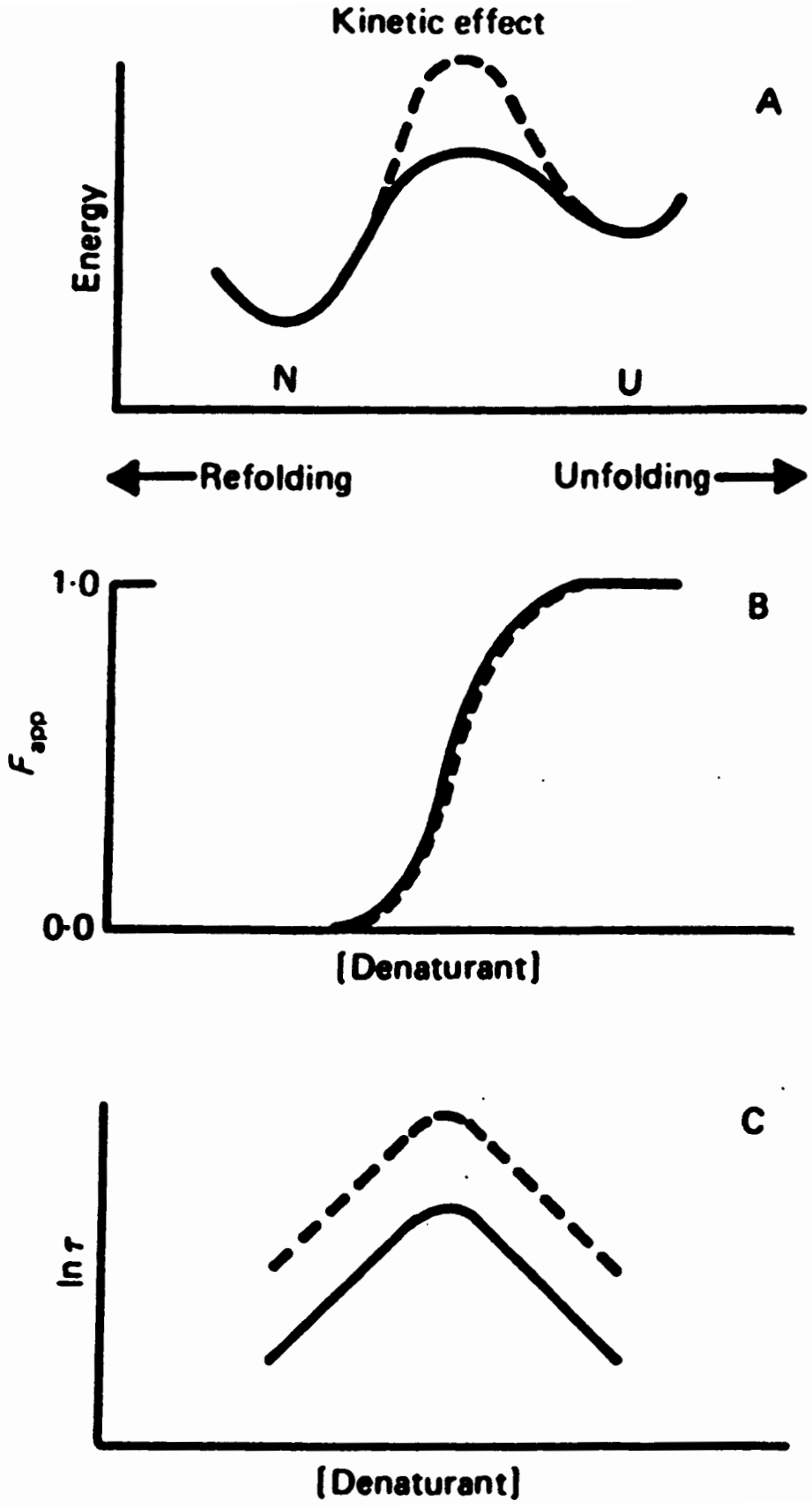
Kinetic effect
A
Energy
N
U
Refolding
Unfolding
1·0
B
F_{app}
0·0
[Denaturant]
C
ln τ
[Denaturant]

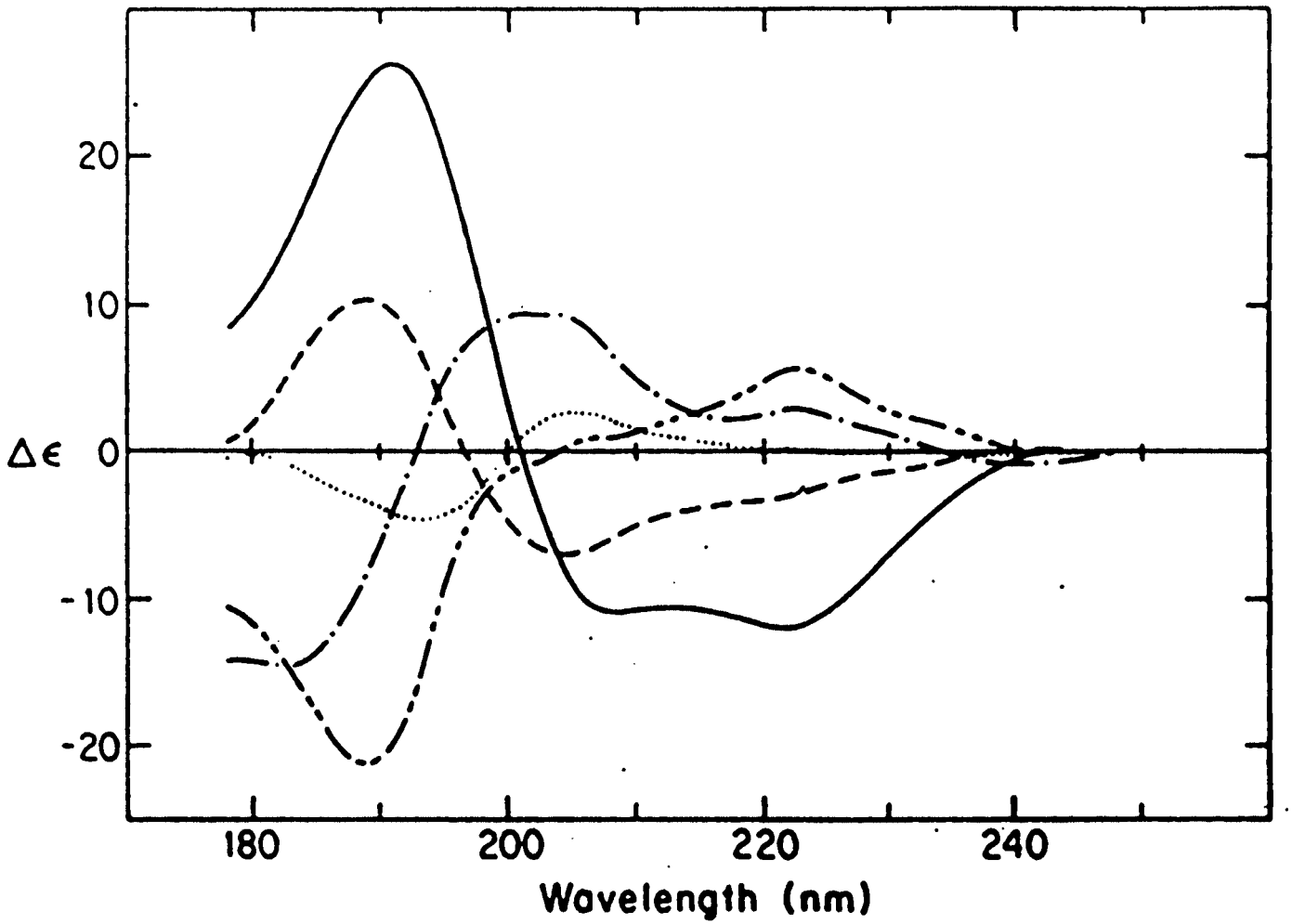

Secondary structure spectra for five major secondary structures from 178 to 260 nm: α-helix (——), antiparallel β-sheet (---), parallel β-sheet (-·-), β-turn (– -- –), other (random) structure (· · ·).

Analysis of a thermal unfolding curve

1. The data are from a thermal unfolding curve determined under the same conditions as the urea unfolding curve analysed in *Table 3*. Values of f_U, K and ΔG were calculated using Equations 2, 3 and 4, respectively. A least-squares analysis of the pre- and post-transition region gave $y_F = 87.2 + 0.66\,(T)$ and $y_U = 646$.

T (°C)	y[a]	f_U	K	ΔG (cal/mol)
16.2	98.1			
21.0	100.9			
25.6	103.7			
30.2	107.4			
45.4	221.3	0.197	0.245	890
46.3	263.9	0.277	0.383	610
47.2	313.9	0.371	0.589	337
48.1	367.6	0.472	0.894	72
49.0	422.2	0.575	1.353	−193
49.9	474.1	0.673	2.061	−464
50.8	518.5	0.757	3.123	−733
51.7	555.5	0.828	4.805	−1013
61.2	645.4			
65.5	646.3			
69.8	646.3			
73.8	645.4			

2. The slope of a plot of ΔG versus $T = -300.3$ cal/mol/deg, and $T = T_m = 48.3$°C at $\Delta G = 0$. Since $\Delta G = 0$ at T_m, $\Delta H_m = (T_m)(\Delta S_m)$. Therefore, $\Delta H_m = (48.3 + 273.2)(300.3) = 96.5$ kcal/mol. The slope of a van't Hoff plot (Equation 6) = −48631 K. Therefore, $\Delta H_m = -(1.987)(-48631) = 96.6$ kcal/mol. The values of ΔH obtained by taking the slope between individual points in the transition regions are: 99.9, 97.5, 94.7, 94.8, 96.7, 96.1 and 100.1 kcal/mol. Clearly, these data cannot be used to determine ΔC_p with Equation 7.
3. To estimate ΔG at 25°C, we use Equation 8. If we assume $\Delta C_p = 0$, the second term in the equation = 0, and $\Delta G(25°C) = 7.0$ kcal/mol. If we calculate ΔC_p using the rough rule of thumb mentioned in the text, ΔC_p = (12 cal/mol/deg/residue) × (104 residues) = 1250 cal/mol/deg. This leads to $\Delta G(25°C) = 7.0 - 1.1 = 5.9$ kcal/mol with Equation 8. Note that this is in excellent agreement with the value of $\Delta G(H_2O) = 5.7$ kcal/mol from the analysis of a urea unfolding curve in *Table 6*.

[a]The value of $-y$ is the specific rotation measured at 295 nm.

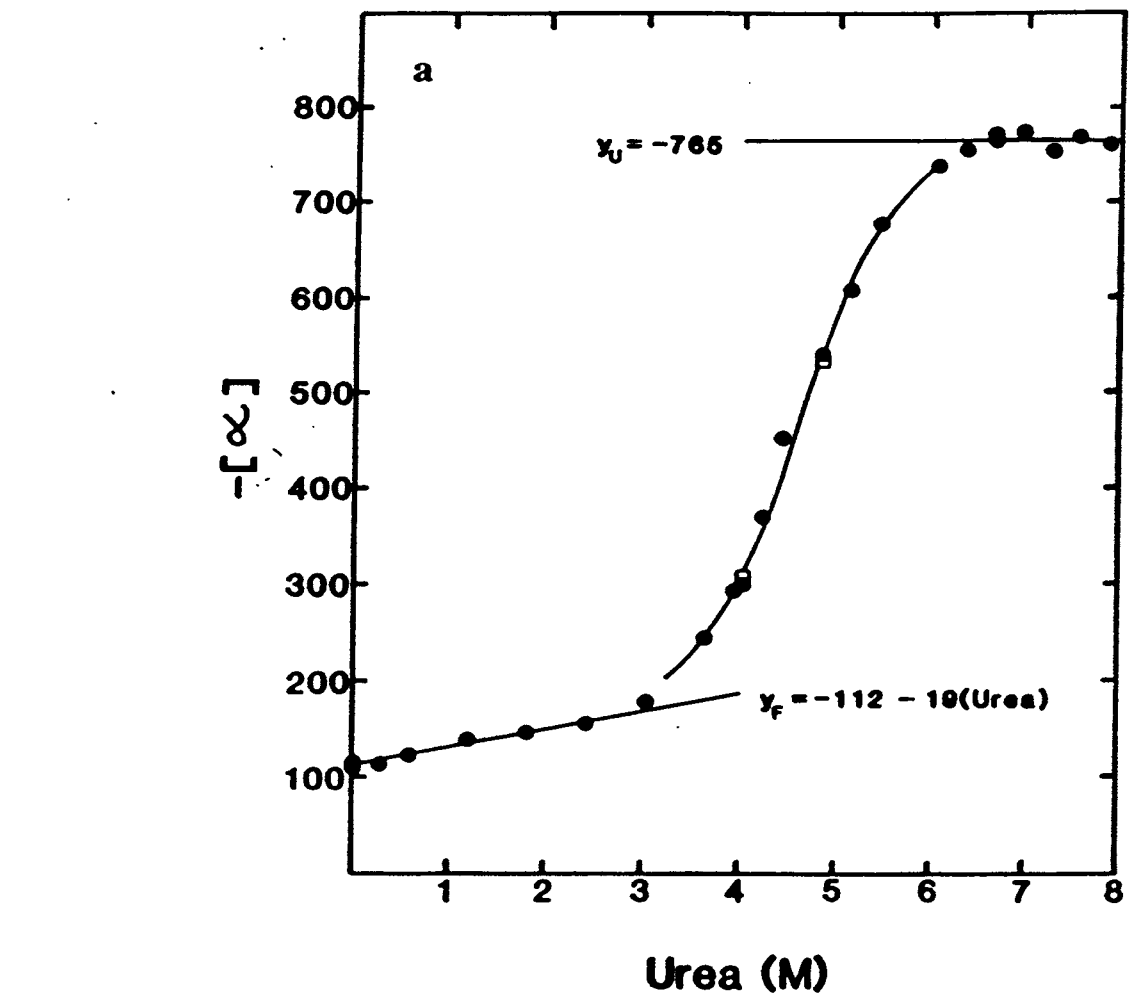
a
800
700
600
500
400
300
200
100
-[α]
$y_U = -765$
$y_F = -112 - 19(Urea)$
1
2
3
4
5
6
7
8
Urea (M)

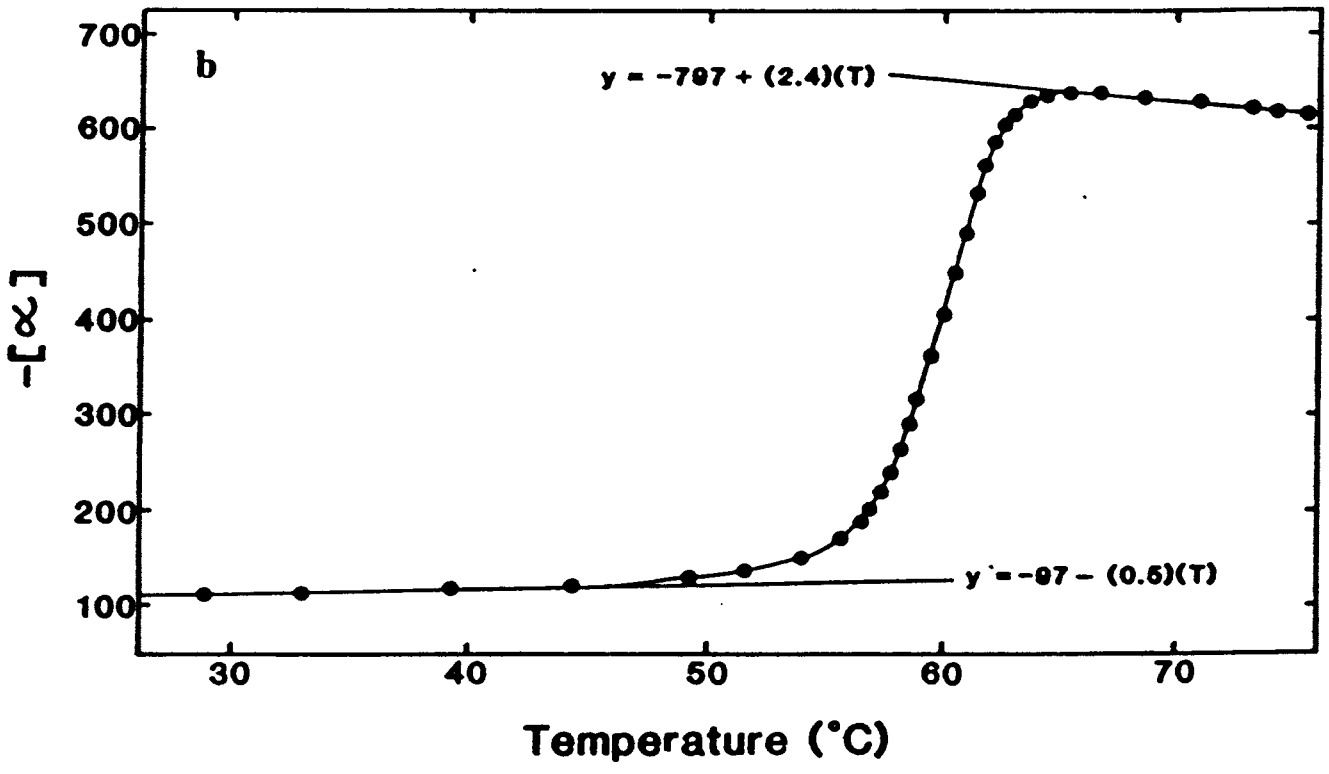
b
700
600
500
400
300
200
100
-[α]
y = -797 + (2.4)(T)
y = -97 - (0.5)(T)
30
40
50
60
70
Temperature (°C)

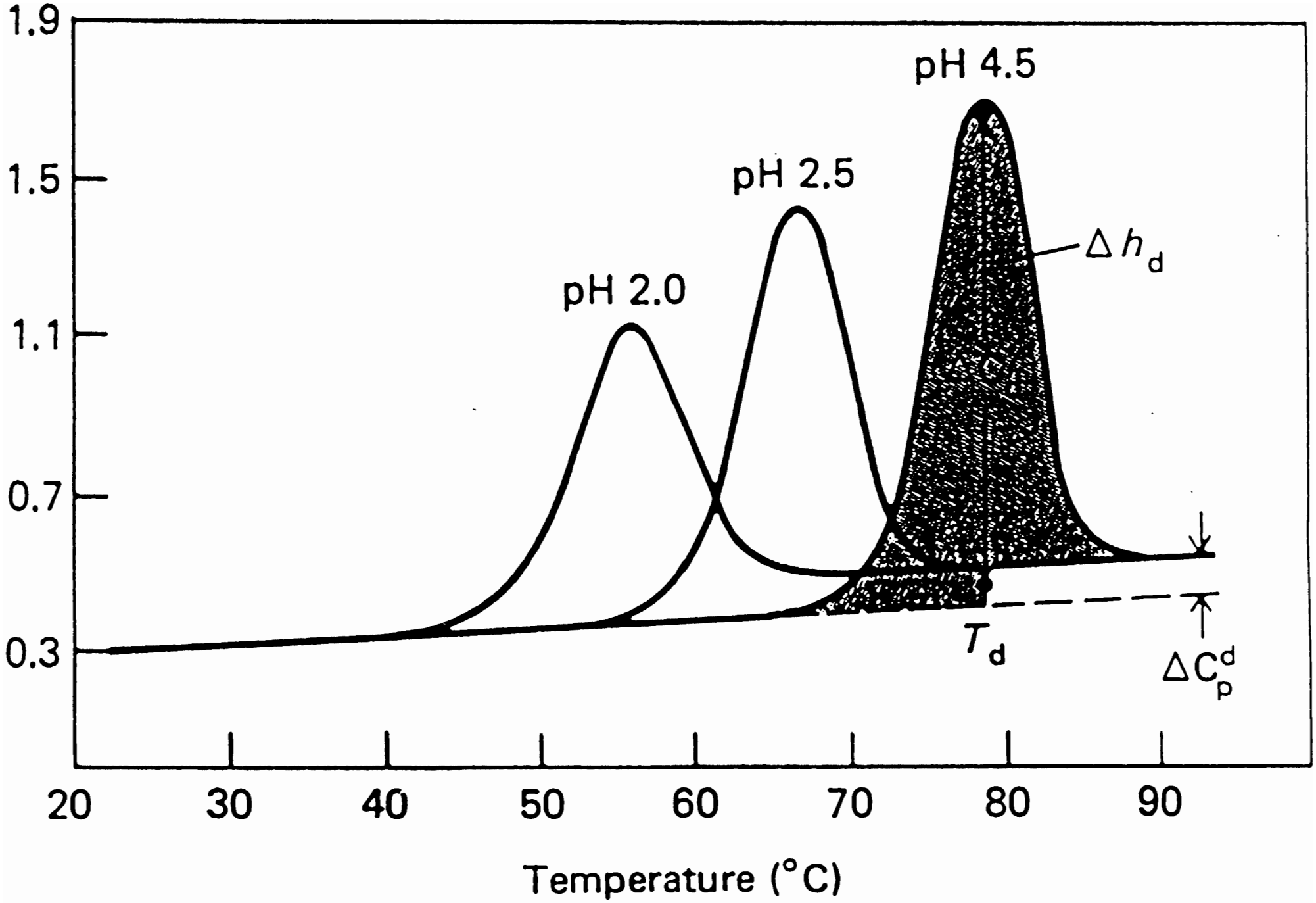
1.9
1.5
1.1
0.7
0.3
pH 4.5
pH 2.5
pH 2.0
Δh_d
T_d
ΔC_p^d
20
30
40
50
60
70
80
90
Temperature (°C)

The stable molten globule

Under mild denaturing conditions several, but by no means all, proteins take up a partially denatured conformation having the following characteristics:

- condensed, with a Stokes radius equal to or not much greater than that of the folded protein
- exhibiting substantial secondary structure, indicated by the far-UV CD spectrum, but with generally reduced stability of the constituent hydrogen bonds
- many side-chains have lost the persistent tertiary interactions of the N state
- the molecule behaves as if 'sticky', consistent with a degree of exposure of non-polar groups to solvent
- if the folded protein is an enzyme, the intermediate is inactive
- an equilibrium transition to the unfolded state suggesting a degree of co-operativity

FIGURE 6–6. Schematic representation of the native and the molten globule states of protein molecules. Nonpolar side chains are hatched.

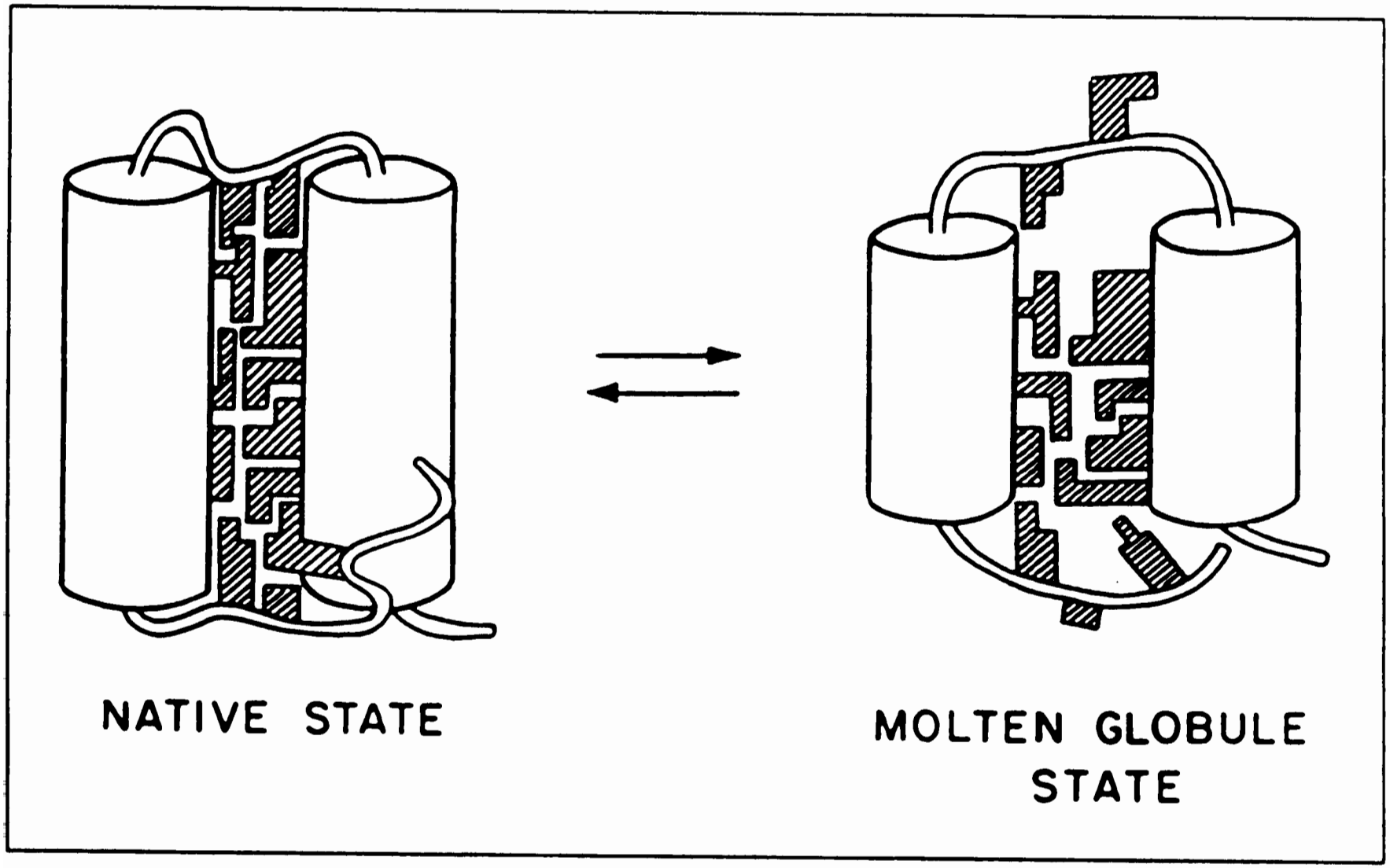

FIGURE 6–6. Schematic representation of the native and the molten globule states of protein molecules. Nonpolar side chains are hatched.

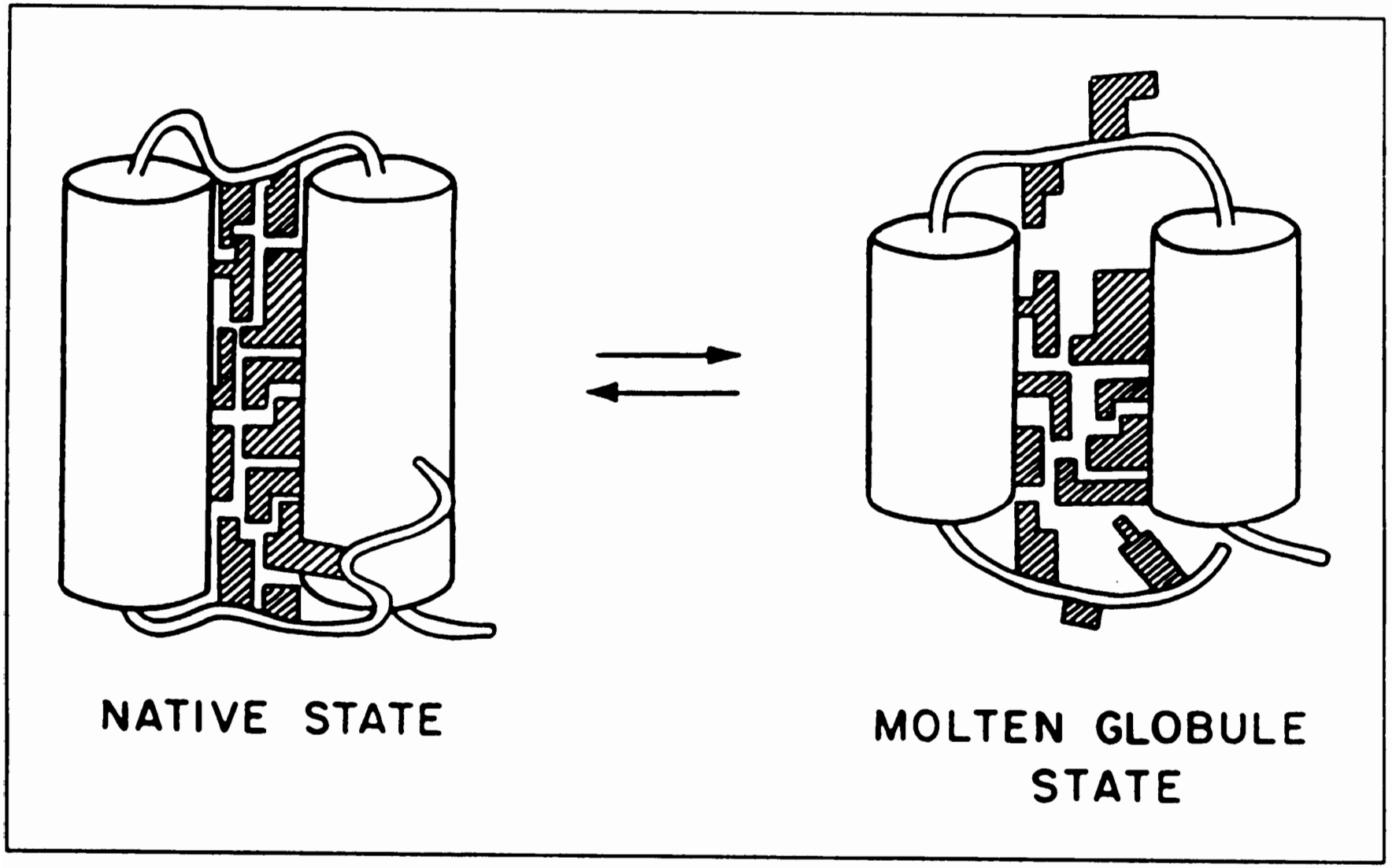

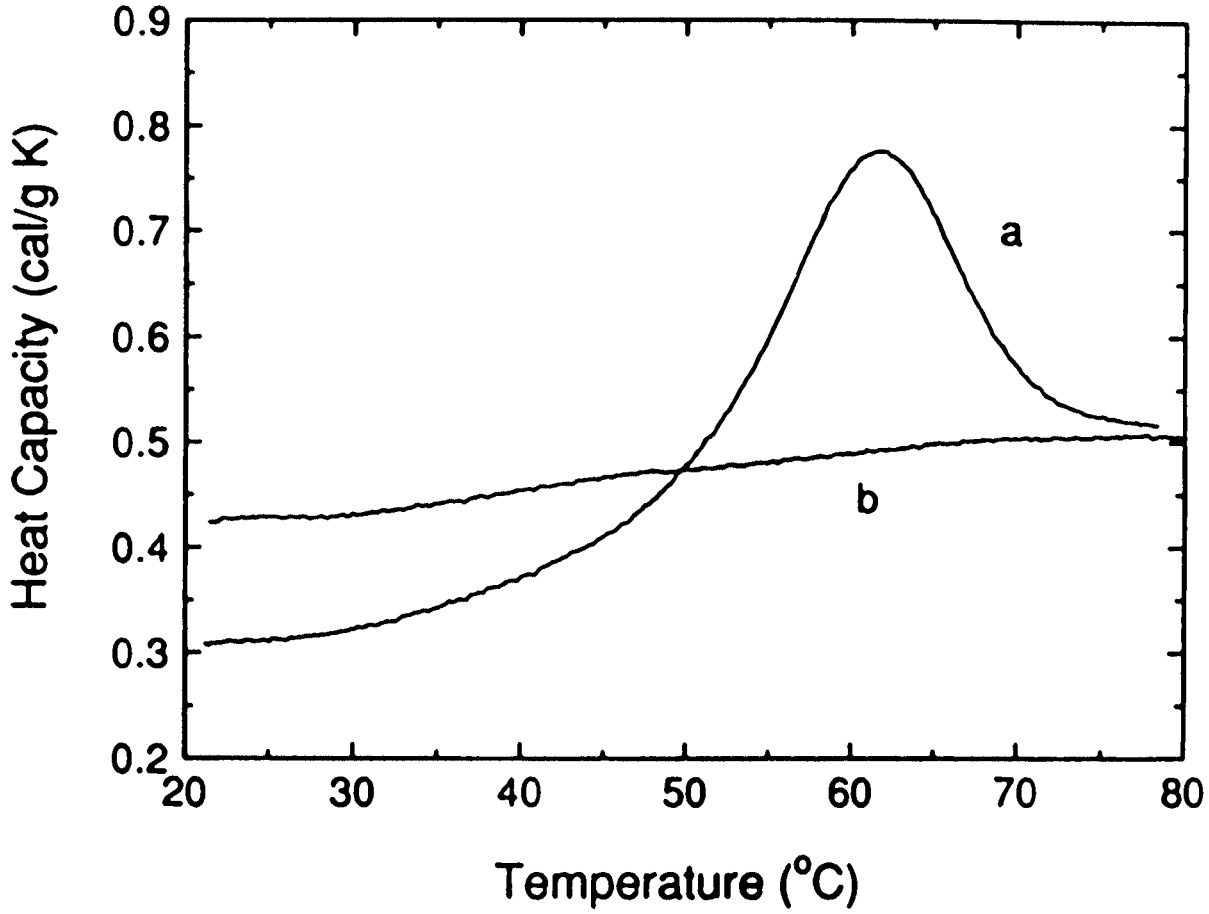

Figure 1. Heat capacity curves of holo-α-lactalbumin and apo-α-lactalbumin. Calorimetry was carried out with DASM4 at the scan rate of 1·0 K/min. Each curve obtained after subtraction of the curve for the dialysis buffer solution as a reference. Curve a: holo-α-lactalbumin (2·14 mg/ml) after dyalisis against 10 mM-borate buffer (pH 8·0). The pH of the solution after heating was 7·8. Curve b: apo-α-lactalbumin (2·48 mg/ml) after dialysis against 10 mM-borate buffer containing 1 mM-EGTA (pH 8). The pH of the solution after heating was 7·6.

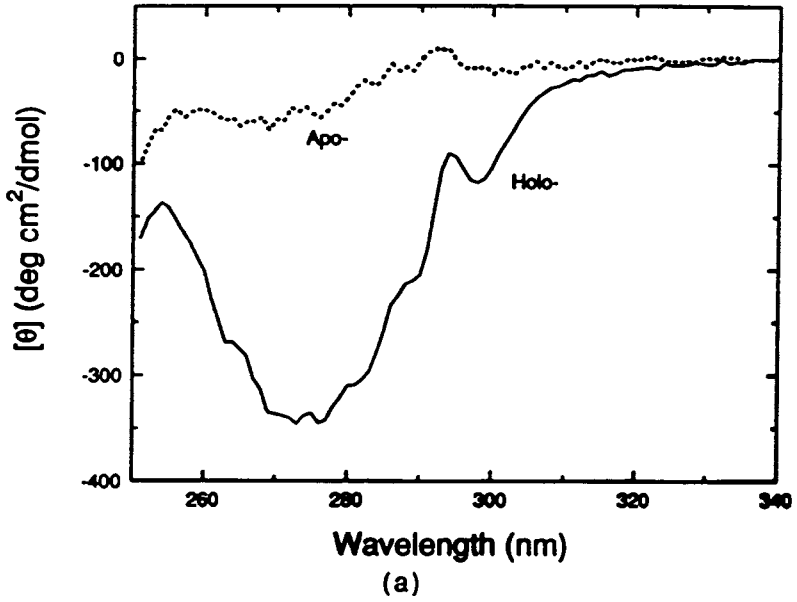

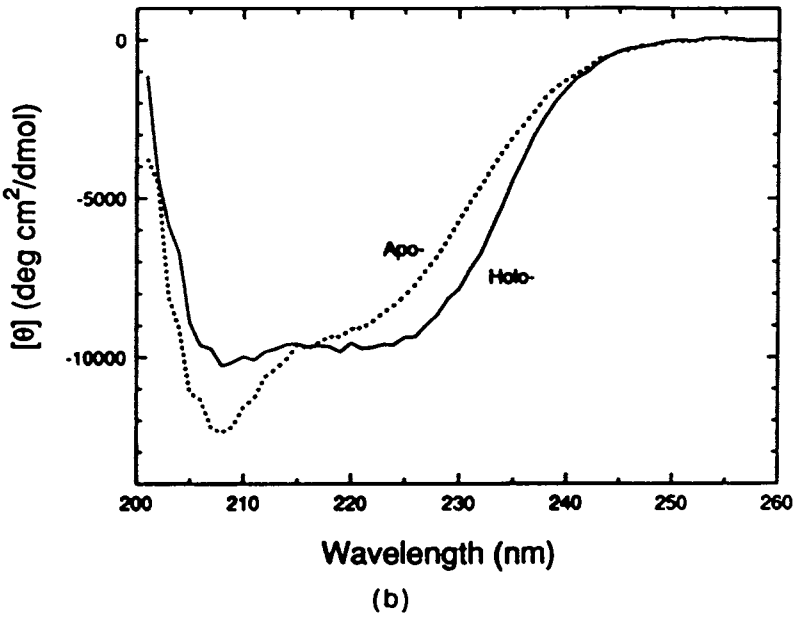

Figure 2. Circular dichroism spectra of holo-α-lactalbumin and apo-α-lactalbumin in the aromatic and far-u.v. regions at 25°C. The c.d. spectra were scanned 16 times at the scan rate of 20 nm/min using a 0·25 s time constant with a Jasco J-500, and the spectra were averaged. For calculation of the mean residue ellipticity, θ, the mean residue weight was taken at 115 for both the proteins. (a) c.d. spectra in the aromatic region were measured at protein concentrations of 0·76 mg/ml for both holo-α-lactalbumin and apo-α-lactalbumin, using a cell with a 10 mm light-path length. The same samples as those for calorimetry were diluted with dialysis buffer. The solutions were at pH 7·7 for holo-protein and at pH 7·6 for apo-protein. (b) c.d. spectra in the far-u.v. region were measured at protein concentrations of 0·41 mg/ml for holo-α-lactalbumin and 0·49 mg/ml for apo-α-lactalbumin, using a cell with a 1 mm path length. The same samples as those for calorimetry were diluted with dialysis buffer. The solutions were at pH 7·5 for holo-protein and at pH 7·6 for apo-protein.

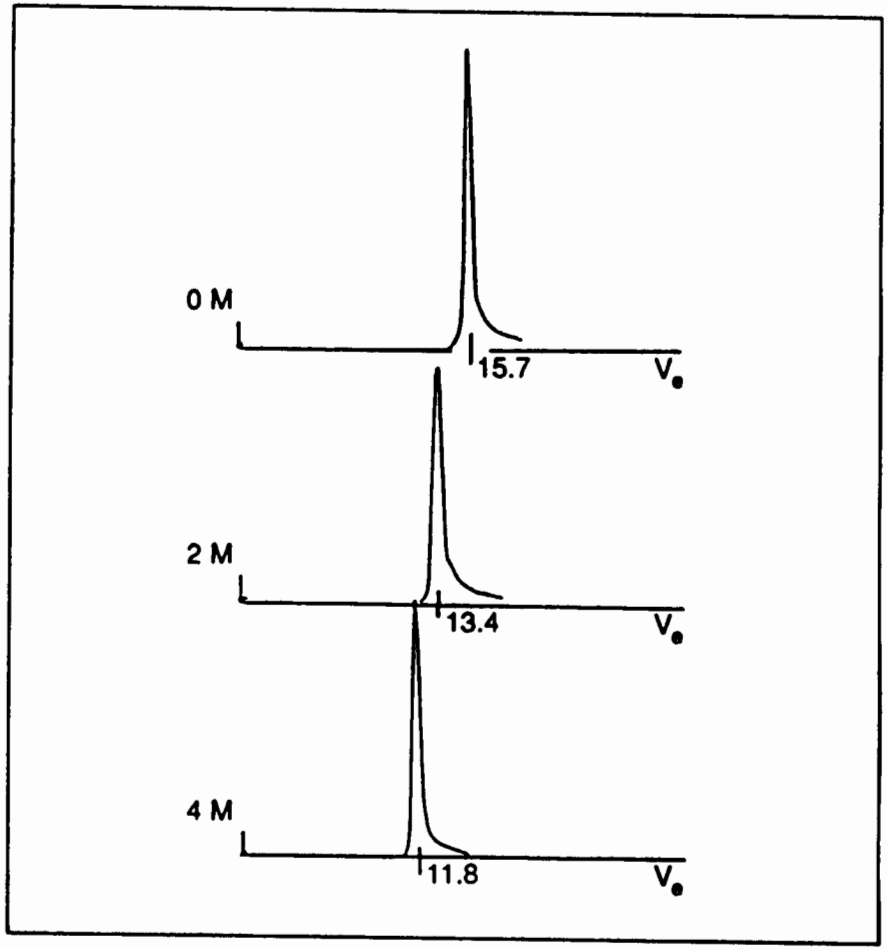

Fig. 2. Size determination of a stable molten globule. Elution profiles are shown for β-lactamase applied in buffer containing the stated concentrations of urea (23). At 2 M urea the protein exhibits the properties of a molten globule (H) and at 4 M is unfolded (U) (14). The values of the elution volume, V_e, are in ml.

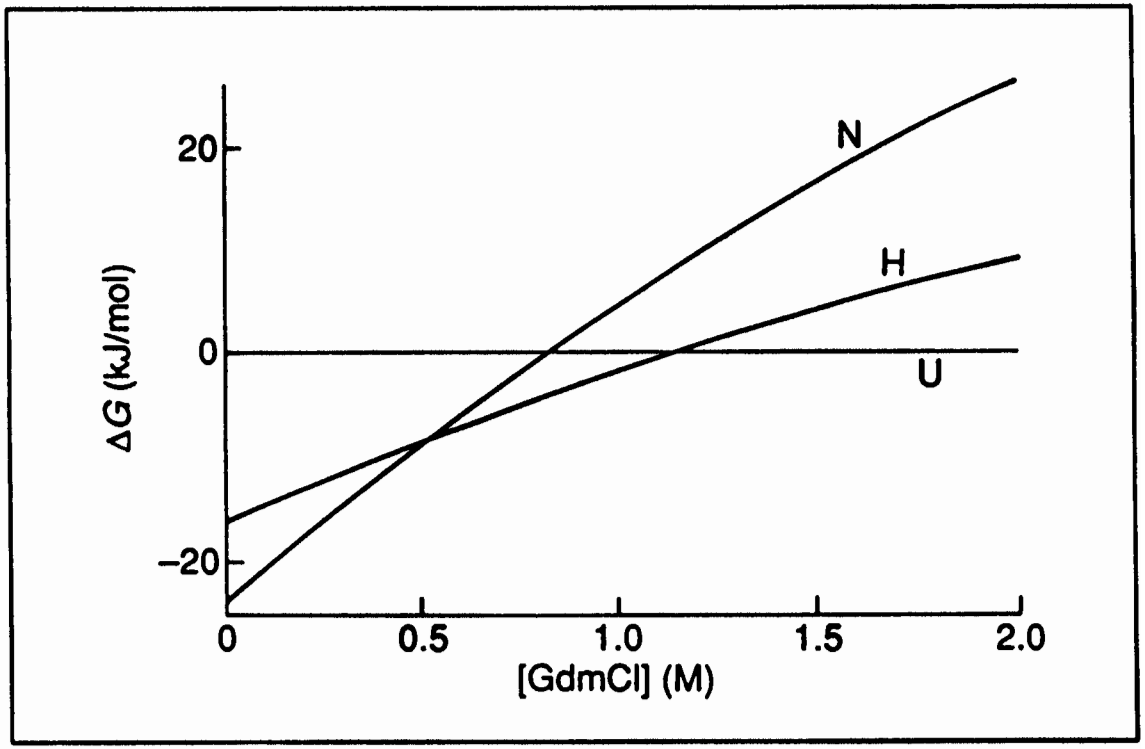

Fig. 5. The free energies of stabilization of the native and intermediate conformers as a function of denaturant concentration. From the three-state denaturation transitions for β-lactamase the free energy differences (equilibrium constants) between the forms were calculated and plotted for the native (N) and molten globule (H) forms, both relative to the unfolded state (35).

The kinetic molten globule

It has been known for a long time that, while native activity and aromatic residue environment frequently recover relatively slowly on refolding, far-UV ellipticity is regained rapidly (35). This points to the accumulation during folding of an intermediate containing secondary structure. Such an intermediate, usually termed I (15, 36), has been identified as the one that precedes the main energy barrier and rate-limiting step in folding:

$$U \xrightarrow{\text{fast}} I \xrightarrow{\text{slow}} N.$$

This intermediate has been the subject of much subsequent research—and discussion!—in the field of protein folding. It has been shown experimentally to:

- be condensed
- contain secondary structure
- have few persistent tertiary interactions
- be 'sticky'
- be inactive (for enzymes)
- be transient, preceding the main rate-limiting step in folding.

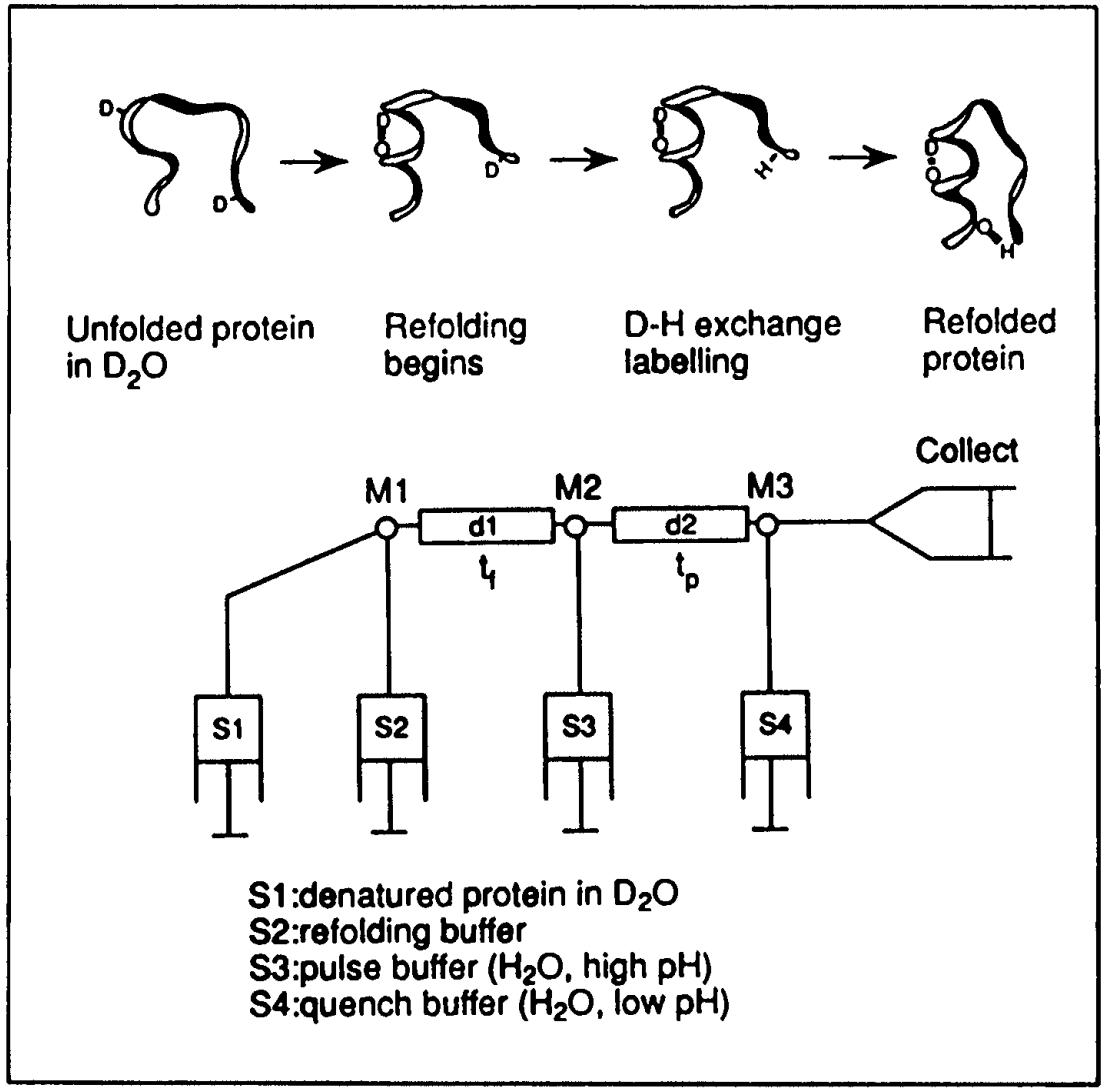

Fig. 1. Schematic illustration of the pulsed hydrogen exchange method. The basic principle is illustrated (*top*) with a hypothetical 'protein' with two representative amide probes. The first ND group becomes protected against exchange in a rapidly forming helical hydrogen bond and remains deuterated, while the second one is still exposed at this time and becomes protonated by D to H exchange during the labelling pulse. A diagram of a quenched-flow apparatus with three mixing stages (M1–M3) and two variable delay lines (d1 and d2) is shown (*below*). Syringes S1 and S2 are activated at t = 0 to initiate refolding by dilution of the denaturant in mixer M1. After a refolding time t_f, the protein solution is mixed in M2 with an H_2O buffer at basic pH (typically pH 9–10) to start the D to H exchange reaction. After a pulse time t_p, exchange is quenched by lowering the pH in M3 under conditions that favour rapid refolding.

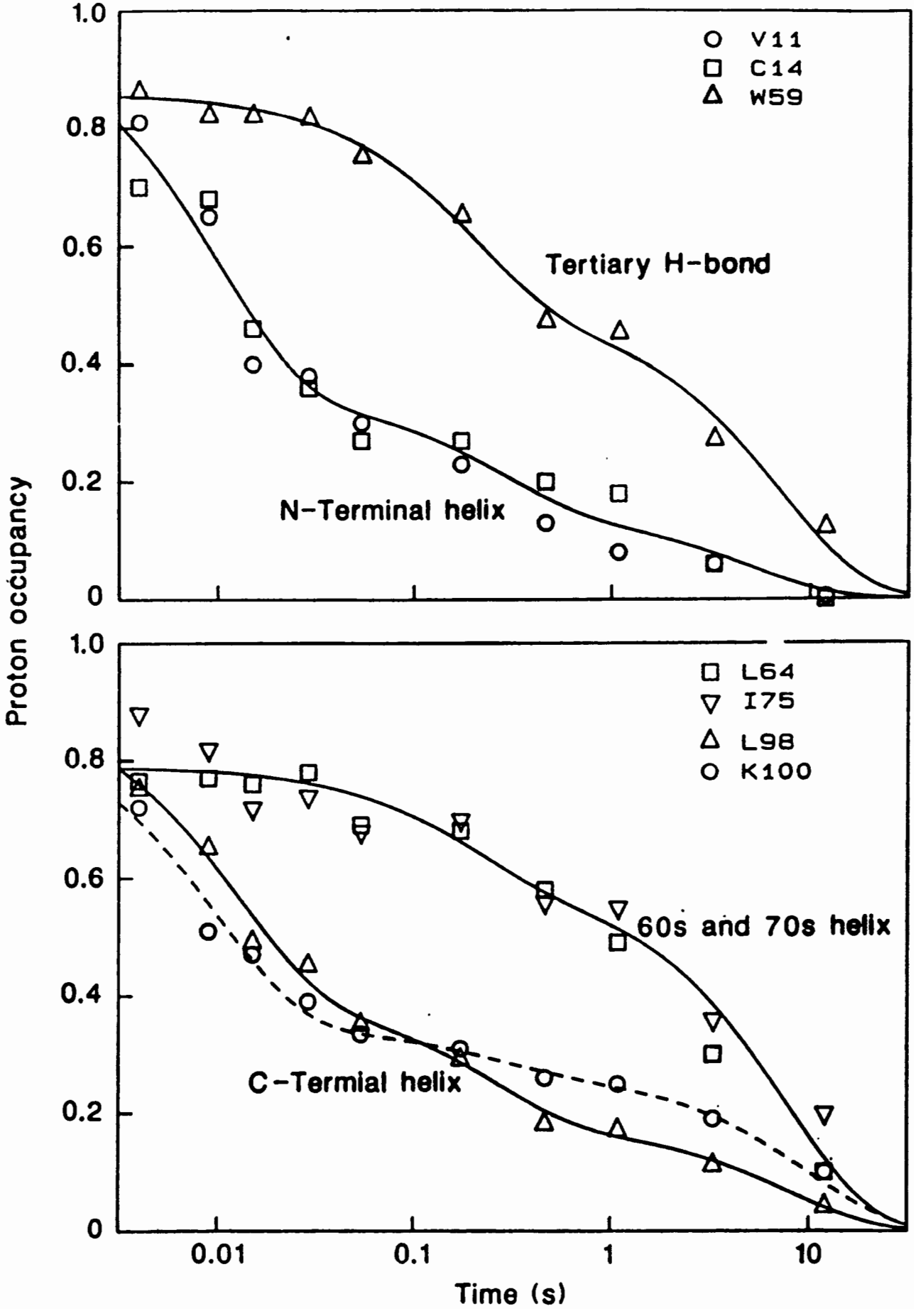
1.0
0.8
0.6
0.4
0.2
0
Proton occupancy
V11
C14
W59
Tertiary H-bond
N-Terminal helix
L64
I75
L98
K100
60s and 70s helix
C-Termial helix
0.01
0.1
1
10
Time (s)

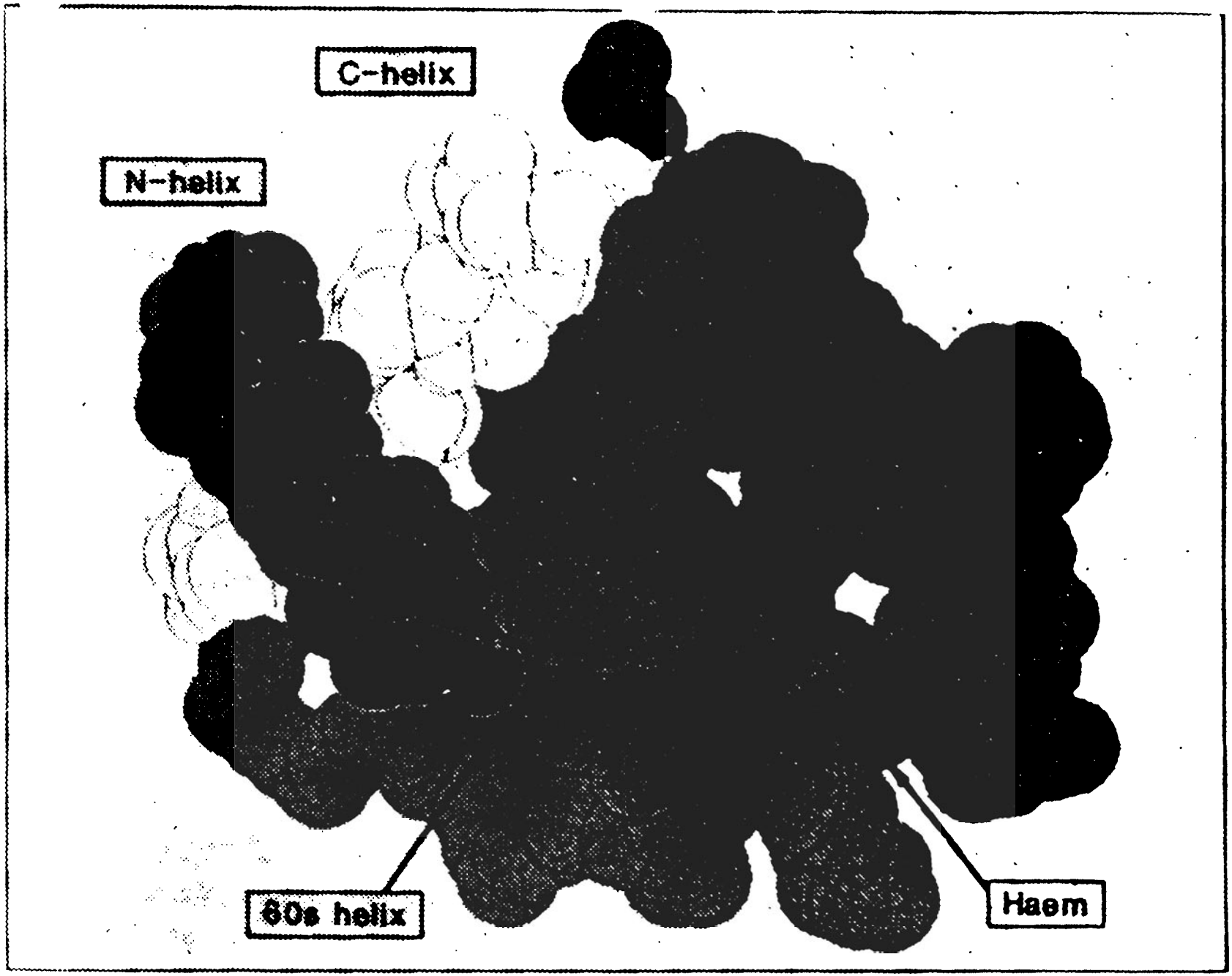

Space-filling model of cytochrome *c*

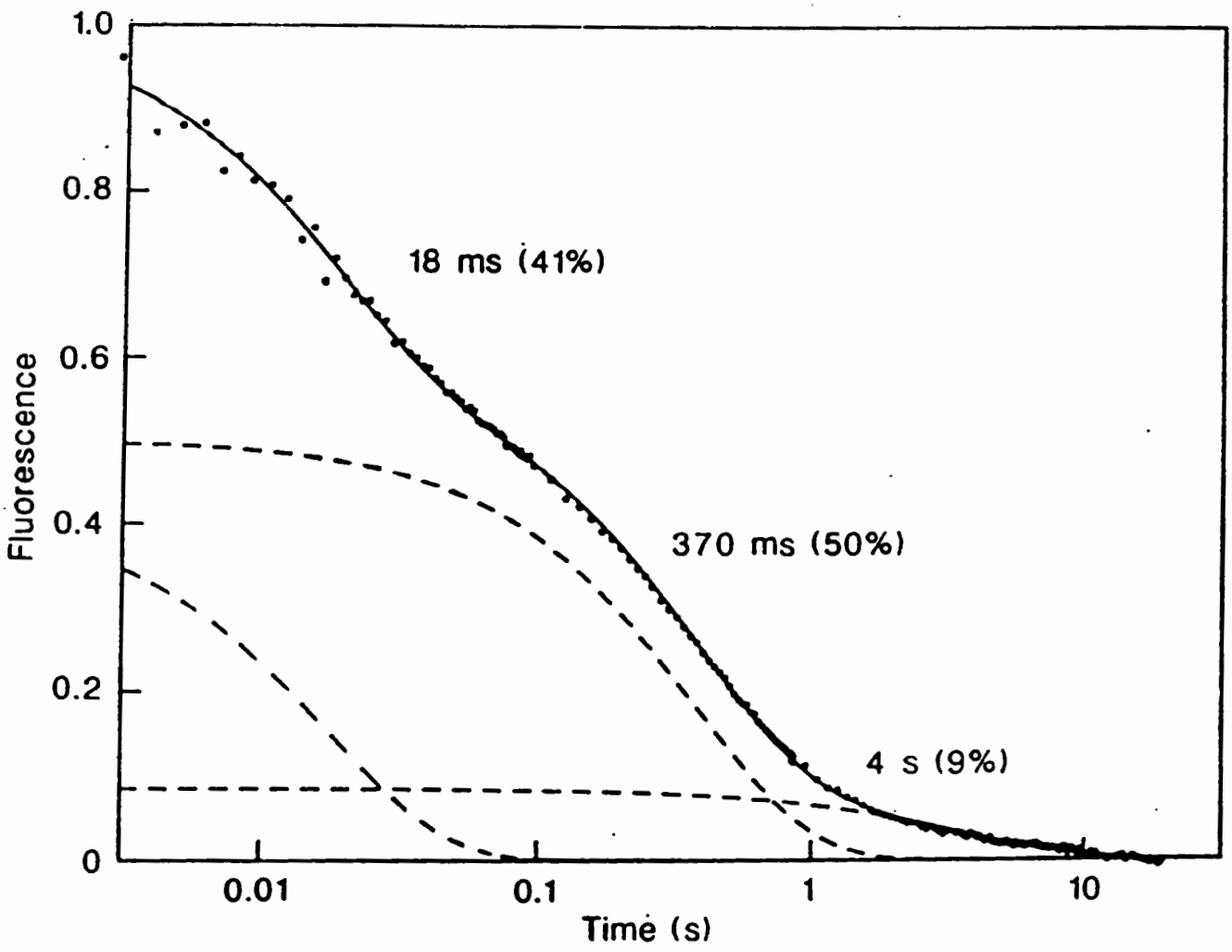

Fig. 4 Refolding kinetics in cytochrome *c* at 10 °C, monitored by the fluorescence of a single tryptophan residue (Trp 59). The data were collected on a Hi-Tech stopped-flow apparatus, using a deuterium lamp for excitation at 280 nm and observation of the fluorescence emission at 350 nm. As in the pulse labelling experiments (Fig. 1), cytochrome *c* was unfolded in 4.2 M GuHCl, *p*H 6.0, and refolded at *p*H 6.2 in the presence of 0.7 M GuHCl. The final protein concentration was 5×10^{-6} M. Under these conditions, unfolding was fully reversible. The kinetic data are presented on the same logarithmic timescale used in Fig. 3. The solid curve was obtained by nonlinear least-squares fitting of three exponential phases, resulting in the indicated time constants and amplitudes. The individual phases are displayed separately with dashed lines.

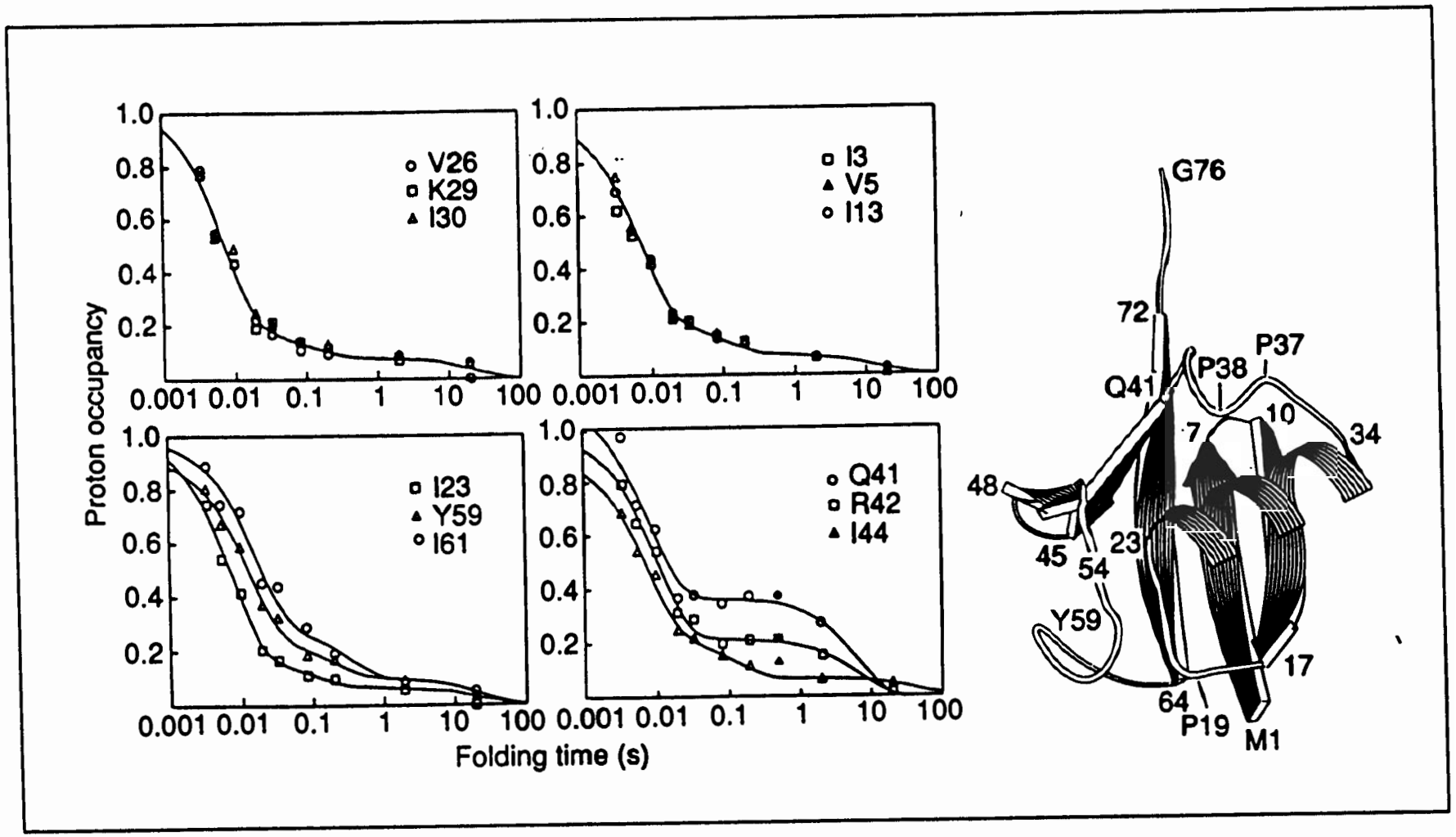

Fig. 6. Time course of amide protection in the folding reaction of ubiquitin (25 °C, pH 5), measured by pulsed hydrogen exchange (75). The proton occupancies for representative amide probes are plotted versus refolding time on a logarithmic scale (1 ms to 100 s). The ribbon diagram shows the backbone structure of ubiquitin. Adapted from ref. 75.

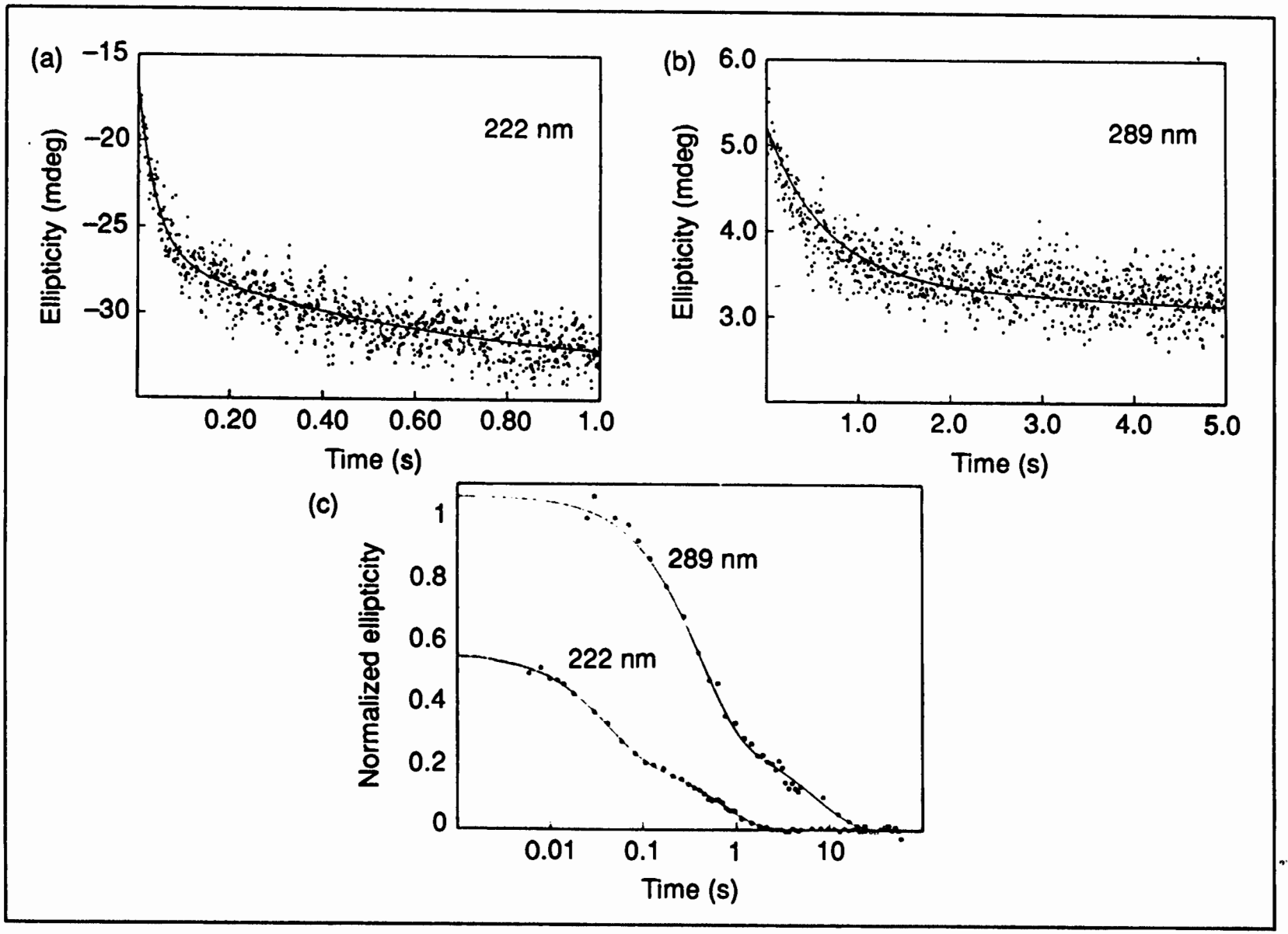

Fig. 3. CD-detected stopped-flow folding kinetics for oxidized cyt *c* at pH 6.3, 10 °C, monitored at 222 nm (a) and 289 nm (b). The folding kinetics at both wavelengths are compared in (c), which shows plots of the normalized ellipticity relative to the fully unfolded state on a logarithmic time-scale. Reprinted from ref. 73, with permission.

Table 1 Relative amplitudes of 'burst phase' measured by time-resolved far-UV CD spectroscopy for various globular proteins

Protein	Amplitude (%)[a]	Dead time (ms)	Reference
α-Lactalbumin	50	20	69
β-Lactoglobulin	200	18	17
Chymotrypsinogen A	100	18	116
Cytochrome *c*	44	4	73
Dihydrofolate reductase	40	18	96
Hen lysozyme	90	4	65,92
Parvalbumin	60	18	97
Rat intestinal fatty acid binding protein	32	~100	115
Ribonuclease T1	100	15	116
Staphylococcal nuclease A	30	15	114
Tryptophan synthase β2	57	13	117
Tryptophan synthase β2 (F2–V8 fragment)	100	4	118

[a] The burst phase amplitude represents the % change in the far-UV CD signal (216–225 nm) occurring in the dead time of the stopped-flow experiment relative to the total change upon refolding.

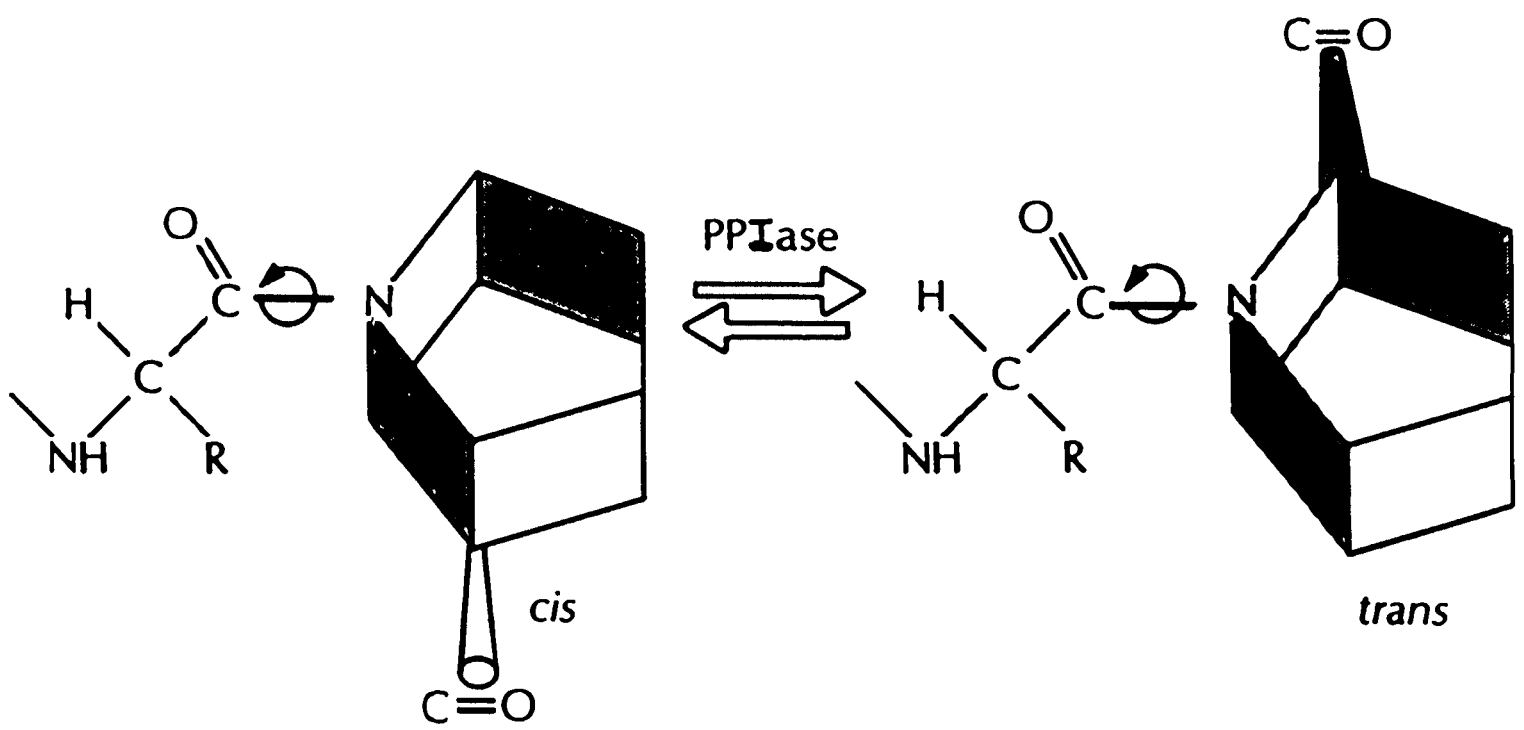
O
H
C
N
NH
R
C=O
cis
PPIase
O
H
C
N
NH
R
C=O
trans

Thiol–disulfide chemistry

Chemical reactions in the formation and trapping of disulfide-bonded folding intermediates. **(a)** Thiol-disulfide exchange between a protein thiolate and a reagent disulfide (RS-SR) to generate a mixed disulfide. **(b)** Intramolecular thiol-disulfide exchange between a protein thiolate and a mixed disulfide which generates a protein disulfide. **(c)** Intramolecular thiol-disulfide exchange between a protein thiolate and an existing protein disulfide to generate a different protein disulfide. **(d)** Protonation of a protein thiolate to generate an unreactive thiol. **(e)** Alkylation of a protein thiol by iodoacetate.

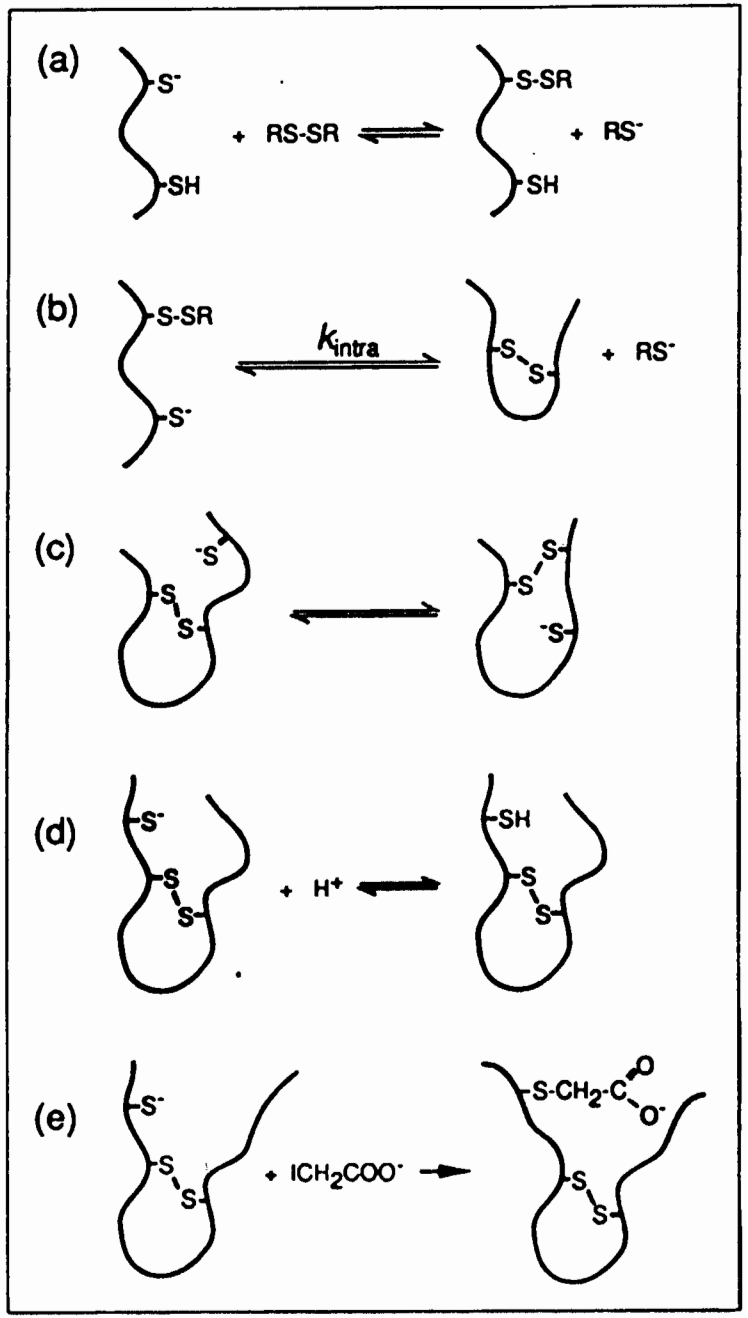

Thiol/disulfide exchange

Disulfide bond formation from two thiols is a two electron oxidation reaction that requires an oxidant. While molecular oxygen (in the presence of trace amounts of heavy metals) may adequately serve this role for some proteins, the most common source of oxidizing equivalents is a low molecular weight disulfide. Protein thiol oxidation to the disulfide results from a thiol/disulfide exchange process (10) that transfers oxidizing equivalents from the low molecular weight disulfide to the protein (eqn 1).

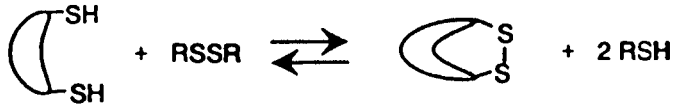

[1]

Thiol/disulfide exchange occurs via direct attack of a nucleophilic thiolate anion on one of the sulfurs of the disulfide bond (eqn 2) (11, 12). The transition state is rather symmetrical with approximately equal bond formation to the nucleophilic sulfur (R_nS^-) and the leaving sulfur ($R_{lg}S^-$) and with a relatively small amount of negative charge on the central sulfur (R_cS) (13).

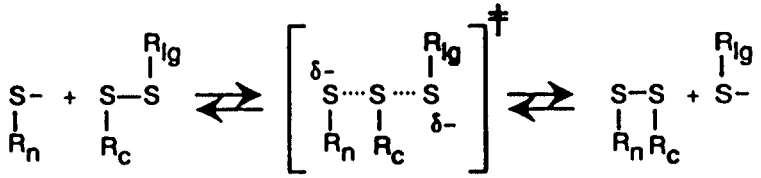

[2]

The rate constant for the reaction increases as the basicity of the attacking thiolate (R_nS^-) nucleophile increases (pK_a increases) and as the basicity of the leaving thiolate ($R_{lg}S^-$) decreases (pK_a decreases). The pK_a of the typical cysteine sulfydryl group is about 8.6; however, this may vary considerably from protein to protein due to the effects of the local environment. At a pH of 8.6, the typical intermolecular step of thiol/disulfide exchange between small molecules or unhindered protein thiols and disulfides will occur with a second-order rate constant of about 20 M^{-1} s^{-1} (14). Since thiol/disulfide exchange occurs via the attack of a nucleophilic thiolate anion, the rate will increase with increasing pH until the attacking thiol is predominantly in the thiolate form.

Protein Disulfide-Isomerase (PDI) accelerates the exchange reactions between disulfide bonds in proteins in the presence of appropriate oxidizing or reducing reagents.

Reaction:

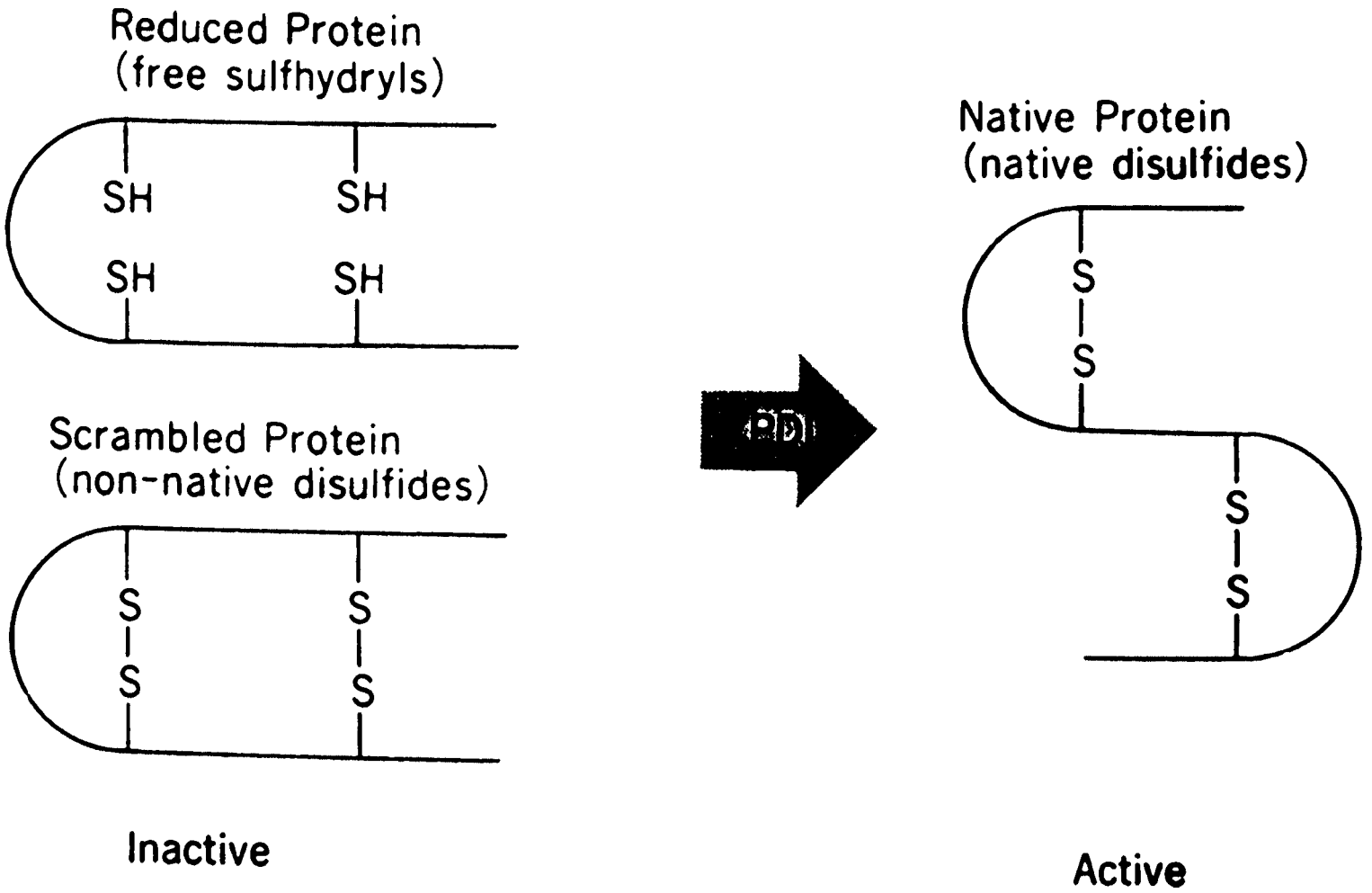

Table 1 Chaperone proteins and their known functions in the cell.

Subcellular location	Organism	Component	Subunit M_r (kDa)	Known functions
The hsp 70 family				
Cytosol	*E. coli*	DnaK	69	Co-operation with the heat shock proteins DnaJ and GrpE in λ DNA replication; activation of RepA for binding to *ori*P1 DNA (86–88); dissociation of protein aggregates (90)
	Yeast	Ssa1–4p	69–72	Stabilization of precursor proteins for translocation into ER and mitochondria (38, 71); binding to nascent polypeptides (72)
	Mammals	hsc70		Uncoating of clathrin-coated vesicles (91)
Mitochondria	Yeast	Ssc1p	70	Membrane translocation, folding of imported proteins (73, 75)
Endoplasmic reticulum	Yeast	Kar2p	78	Protein translocation into the ER; assembly within the ER (31); retention of misfolded proteins (29, 79)
		BiP, Grp78	70	
The hsp60 family				
Cytosol	*E. coli*	GroEL	58	Folding of monomeric and multi-subunit proteins (102, 103, 109–113, 116, 118)
		GroES	10	
Mitochondrial matrix	Fungi, mammals	hsp60, hsp58	58–64	Folding and assembly of newly imported proteins (75, 101)
		hsp10	10	
Chloroplasts	Plants	Rubisco subunit binding protein	61 (α-chain) 60 (β-chain)	Folding and assembly of rubisco and probably of other proteins imported into chloroplasts (151)
SecB	*E. coli*		17	Stabilization of precursor proteins for export across the cytoplasmic membrane (45, 127)
The hsp90 family				
Cytosol	Mammals	hsp90	90	Stabilization of steroid hormone receptors in a conformation competent to bind hormone (139); association with $pp60^{src}$ before its phosphorylation (134); facilitation of refolding by preventing aggregation (143)

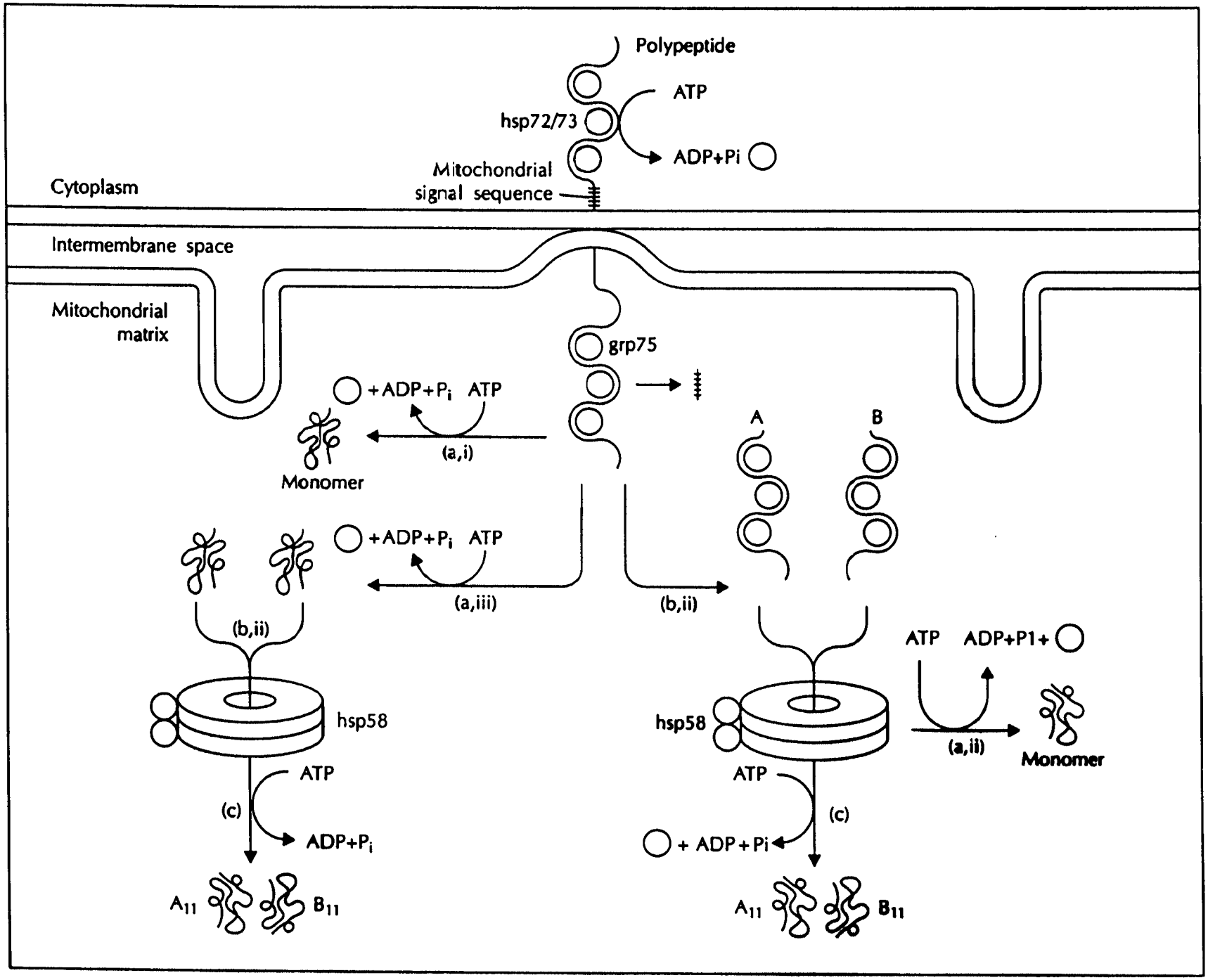
Polypeptide
ATP
hsp72/73
ADP+Pi
Mitochondrial
signal sequence
Cytoplasm
Intermembrane space
Mitochondrial
matrix
grp75
+ADP+Pi ATP
(a,i)
Monomer
A
B
+ADP+Pi ATP
(a,iii)
(b,ii)
(b,ii)
ATP ADP+P1+
hsp58
hsp58
(a,ii)
Monomer
ATP
ATP
(c)
(c)
ADP+Pi
+ ADP+Pi
A11
B11
A11
B11

'The *in vivo* folding problem', or 'Out of the ribosome, into the jungle'